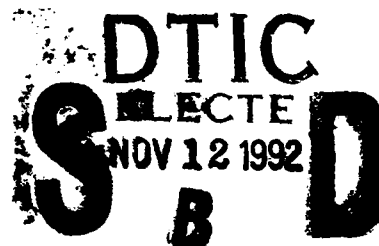# A TRIDENT SCHOLAR
PROJECT REPORT

NO. 188

"Investigation of Antarctic Sea
Ice Concentration by Means
of Selected Algorithms"

AD-A257 132

UNITED STATES NAVAL ACADEMY
ANNAPOLIS, MARYLAND

92-29346

"Investigation of Antarctic Sea
Ice Concentration by Means
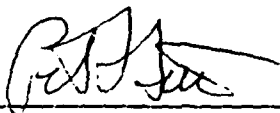of Selected Algorithms"

A Trident Scholar Project Report

by
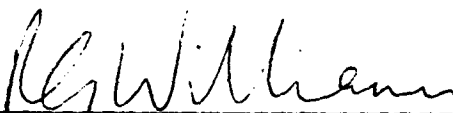
Midshipman Andrew S. Lomax, Class of 1992

U.S. Naval Academy
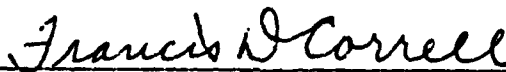
Annapolis, Maryland

_____

Associate Professor Peter L. Guth
Oceanography Department

_____

Visiting Professor Robin G. Williams
Oceanography Department

Accepted for Trident Scholar Committee

_____
Chair

_____
8 May 1992
Date

USNA-1531-2

REPORT DOCUMENTATION PAGE

Public reporting burden for this collection of information is estimated to average 1 hour per response, including the time for reviewing instructions, searching existing data sources, gathering and maintaining the data needed, and completing and reviewing the collection of information. Send comments regarding this burden estimate or any other aspect of this collection of information, including suggestions for reducing this burden, to Washington Headquarters Services, Directorate for Information Operations and Reports, 1215 Jefferson Davis Highway, Suite 1204, Arlington, VA 22202-4302, and to the Office of Management and Budget, Paperwork Reduction Project (0704-0188), Washington, DC 20503

1. AGENCY USE ONLY (Leave blank)	2. REPORT DATE 8 May 1992	3. REPORT TYPE AND DATES COVERED Final 1991/92

4. TITLE AND SUBTITLE
INVESTIGATION OF ANTARCTIC SEA ICE CONCENTRATION BY MEANS OF SELECTED ALGORITHMS

5. FUNDING NUMBERS

6. AUTHOR(S)

Lomax, Andrew S.

7. PERFORMING ORGANIZATION NAME(S) AND ADDRESS(ES)

U.S. Naval Academy, Annapolis, Md.

8. PERFORMING ORGANIZATION REPORT NUMBER

U.S.N.A. - TSPR;
188 (1992)

9. SPONSORING/MONITORING AGENCY NAME(S) AND ADDRESS(ES)

10. SPONSORING/MONITORING AGENCY REPORT NUMBER

11. SUPPLEMENTARY NOTES

Accepted by the U.S. Trident Scholar Committee

12a. DISTRIBUTION/AVAILABILITY STATEMENT

This document has been approved for public release; its distribution is UNLIMITED.

12b. DISTRIBUTION CODE

13. ABSTRACT (Maximum 200 words)

Changes in areal extent and concentration of sea ice around Antarctica may serve as sensitive indicators of global warming. A comparison study was conducted between the outputs of the three main algorithms currently in use (NASA Team, Comisco, and NORSEX) and a sea-ice model (Fine Resolution Antarctic Model). Data from the DMSP Special Sensor Microwave/Imager (SSM/I) were used as input algorithms for the time frame July, 1987 to June, 1990. Large disparities are apparent when comparing the NASA algorithm with the Comisco and NORSEX algorithms. Very large differences, some higher than 30 per cent, exist in the marginal ice zones, along the coast, and in the Weddell and Ross Seas Heat fluxes through recurring polynyas were claculated to quantify further differences in the algorithms; however, no conclusive patterns were apparent. No significant change in the extent or area of the ice pack occurred from July, 1987 through June, 1990.

14. SUBJECT TERMS

Antarctic Ocean; Antarctic regions; global warming; Sea ice - Antarctic regions

15. NUMBER OF PAGES
99

16. PRICE CODE

17. SECURITY CLASSIFICATION OF REPORT	18. SECURITY CLASSIFICATION OF THIS PAGE	19. SECURITY CLASSIFICATION OF ABSTRACT	20. LIMITATION OF ABSTRACT
UNCLASSIFIED	UNCLASSIFIED	UNCLASSIFIED	

Abstract

Changes in areal extent and concentration of sea ice around Antarctica may serve as sensitive indicators of global warming. These parameters are routinely estimated from satellite-derived passive microwave data by applying conversion algorithms to measured brightness temperatures. A comparison study was conducted between the outputs of the three main algorithms currently in use (NASA Team, Comiso and NORSEX) and a sea-ice model (Fine Resolution Antarctic Model). Data from the Defense Meteorological Satellite Program (DMSP) Special Sensor Microwave/Imager (SSM/I) were used as input to the algorithms for the time frame July, 1987 to June, 1990. The Comiso and variable-temperature NORSEX algorithms predict very similar ice concentrations (< 5% difference). Differences as great as 15% do exist, though, in the marginal ice zone and in regions of coastal polynyas with the NORSEX algorithm giving higher values. Large disparities are apparent when comparing the NASA algorithm with the Comiso and NORSEX algorithms. Very large differences, some higher then 30%, exist in the marginal ice zones, along the coast, and in the Weddell and Ross Seas. Heat fluxes through recurring polynyas were calculated to quantify further differences in the algorithms; however, no conclusive patterns were apparent. No significant change in the extent or area of the ice pack occurred from July, 1987 through June, 1990.

Acknowledgments

I owe several people a great deal of thanks for helping in the completion of this project. First and foremost, I would like to thank Associate Professor Peter Guth, my principal advisor, for his guidance, programming expertise, and patience with my MS-Dos/Pascal ignorance. Visiting Professor Robin Williams from the Scott Polar Research Institute, University of Cambridge in England provided unlimited ideas, advice, and contacts. I would also like to thank Drs. J.C. Comiso, D.J. Cavalieri and Robert Massom of the Laboratory for Hydrospheric Sciences, NASA/Goddard Space Flight Center for their advice and guidance.

The brightness temperature gridded data used in the project were supplied by the National Snow and Ice Data Center and the NASA/Goddard Space Flight Center. I also want to thank Beverly de Cuevas and Tim Hateley of the Institute of Oceanographic Sciences, Deacon Laboratory for providing the FRAM data. A FORTRAN program of the NORSEX algorithm and supporting documentation were supplied by Kjell Kloster of the Nansen Remote Sensing Center, Norway.

Appreciation is also in order for my parents and brother for their understanding and words of encouragement. Most importantly, I want to thank my fiancee, Rebecca Freet, for her patience and encouragement during the stressful times and for understanding when the project needed to take priority.

Table of Contents

List of Figures

List of Tables

Introduction

Mankind has long had an interest in the Antarctic region. Explorers searched for centuries for the southern continent believed to exist since the time of the ancient Greeks and Romans. The first sighting of the continent occurred around 1820 though the actual person to make the sighting is disputed. The first landing on Antarctica did not take place until 1895, and soon after began the race to the South Pole. Roald Amundsen, the great Norwegian explorer, was the first man to reach the South Pole in 1911. Since that time, hundreds of expeditions, experiments, and research establishments have occurred in and around Antarctica.

Antarctica has also been an area of commercial interest. Throughout the 1800's, oil companies sent their ships to the Southern Ocean to exploit the abundance of whales and seals. The harvesting of krill and fish has also been a source of income for several countries. Antarctica is believed to contain a wealth of mineral and petroleum resources; however, the retrieval of such resources has been limited by agreements in the Antarctic Treaty.

Perhaps the most prominent portion of man's interest in Antarctica has been in the area of scientific investigation. The polar regions, particularly Antarctica, are important components of the worldwide ecosystem in several respects.

The Southern Ocean is unique in that it is the only conduit between the world's major oceans. As a result, this region plays a major role in meridional heat transport and, therefore, the global climate. Because the continent is isolated from warm water by the cold ocean surrounding it, a massive glacial build-up has covered Antarctica over several million years. This glacial build-up makes Antarctica integral to the global hydrologic cycle as it contains the bulk of the world's freshwater. The polar regions are also important to the global carbon dioxide cycle, acting as sources in winter and spring and sinks in summer. In addition, the polar regions could act as early indicators of carbon dioxide-induced global warming. Models suggest that a warming trend in the lower latitudes would be magnified several times in the polar regions because of their role as heat sinks [*Zwally et al.*, 1983]. One method of detecting this warming trend would be a significant decrease in the sea-ice coverage over a long period of time. Antarctica has also become an area of intense interest because of the depletion of the ozone layer over the continent. Because it plays a key role in many global oceanographic and atmospheric processes, a great deal of scientific research has been and will be devoted to the Antarctic environment.

The gathering of scientific data in and around Antarctica have always been extremely difficult because of the environmental conditions. Frigid temperatures, high winds, and rough seas make the Southern Ocean a formidable

habitat. Early techniques relied on shipborne measurements for data gathering. As technology increased, so too have the quality, quantity, and span of Antarctic data sets. Buoys have eliminated the need for human participation in data gathering though there is no control over where the buoys drift. However, the most important technological development in the realm of polar data gathering has been the advent of remote sensing from satellites. Satellites have provided both large- and small-scale views of the polar regions at a considerably larger spatial and temporal scale and at a fraction of the cost of similar shipborne measurements.

The original objectives of this research project included: (1) to gather and organize data for Antarctic sea-ice extent and sea-ice area from the years 1973 to present, (2) to compare the results of data calculated by means of several existing algorithms, (3) to develop an animated display of the growth and ablation of Antarctic sea ice, and (4) to make observations of the overall trend of sea-ice cover during the aforementioned time period with special attention to signs of global warming. During the course of the year, two additional objectives were pursued; namely: (5) to determine the turbulent heat losses through several recurring polynyas in an effort to quantify differences between algorithm results and (6) to compare observed sea-ice concentration values from satellite data to values generated by a numerical model.

Due to unforeseen circumstances several of these objectives were not fully attainable. Satellite data from 1973 through June 1987 were not available until mid-April, thus reducing the span of analysis to July 1987 through June 1990. This severely hampered the ability to determine the presence of long-term decrease in the sea-ice coverage. A quantitative comparison between model output and satellite observations was not possible because of problems with the model data to be discussed later.

Stages of Sea-ice Growth

Very little work has been devoted to the study of sea ice in its natural environment. This stems from the remote location, harsh conditions, and expense of this type of work. Observations from the well-studied development of freshwater ice are used to gain an understanding of similar processes in sea ice.

Freshwater freezes at a temperature of 0°C; however, the presence of dissolved solids in sea water reduces the freezing point to approximately -1.9°C. Because freezing is a change of phase, the water must become supercooled to overcome the heat of fusion. The precise amount of supercooling necessary to initiate ice formation has not been studied but it is believed to be a few hundredths or tenths of a degree Celsius [Weeks and Ackley, 1986]. Therefore, it can be said that sea ice with a salinity of 35 ppt will

freeze at a temperature between -1.9 and -2.0°C. Ice initially forms disc-shaped crystals approximately 2-3 mm in diameter. In the absence of wind, waves, currents, and other external disturbances, these crystals will form a smooth unbroken surface of sheet ice as described in *Weeks and Ackley* [1986]. However, the oceans are in a constant state of turbulence and the initial stages of sea-ice growth are not structured processes. These disc-shaped crystals, commonly called frazil ice, are the building blocks of further ice development.

The accumulation of frazil results in one of two ice types: grease ice and pancake ice. Grease ice, a thick, soupy mass of frazil, earned its name because of the dark, matte appearance of the ice. Grease ice is distinguished from more compact agglomerations of frazil by its viscous, fluid-like properties [*Weeks and Ackley*, 1986]. The second product of frazil ice occurs when the individual crystals are bonded together by wave action to form circular pieces of consolidated pancake ice. These pancakes are characterized by slightly upturned edges due to the constant collisions between the pancakes. Pancake ice can form directly from frazil or it can result from consolidation of grease ice. The space between individual pancakes normally contains open water or grease ice. The pancakes eventually join to create a solid sheet of ice. The aforementioned ice types are categorized as new ice - any ice with a thickness up to 10 cm [*Stringer et al.*, 1984].

Once the initial sheet is formed, the ice growth proceeds in a downward direction driven by the heat lost to the atmosphere. This stage of growth is called young ice and ranges from 10 to 30 cm in thickness. The downward growth of ice is called "columnar ice" because of the column-like arrangement of the crystals. Young ice is gray in color because it is still thin enough for the underlying water to reduce its albedo.

First-year ice describes ice with a thickness greater than 30 cm. Ice remains first-year ice until it melts or it survives a summer melt season. First-year ice has a very high albedo because it is thick enough to reduce the effects of the underlying water and is white in appearance. The thickness of first-year ice rarely exceeds 2 meters without deformation but can reach thicknesses of 20 m from the formation of pressure keels [Parkinson et al., 1984]. Ice that has survived a melt season is termed multiyear ice and is substantially different from first-year ice in appearance and structure. Multiyear ice has a much lower salinity than first-year ice and has a rolling, hummocky surface.

The mechanical, thermal, and electromagnetic properties of sea ice strongly depend on the salinity of the ice. During the formation of ice crystals, dissolved solids are rejected. However, if the ice forms rapidly, pockets of brine will be trapped in the ice structure. The presence of brine pockets in the ice dampens the thermal conductivity of the ice, mechanically weakens the ice, and also reduces

electromagnetic optical depth of the ice. As sea ice ages, its salinity decreases with brine drainage and brine flushing accounting for the bulk of the desalinization [*Gow and Tucker*, 1990]. As the ice sheet grows thicker, its surface rises higher above sea level to maintain isostatic equilibrium. This creates a pressure head within the interconnected brine system and the brine drains out of the ice into the underlying ocean [*Gow and Tucker*, 1990; *Weeks and Ackley*, 1986]. Brine flushing is a process similar to drainage except that the hydrostatic head from the surface meltwater drives the pressure head that forces the brine out [*Gow and Tucker*, 1990; *Weeks and Ackley*, 1986]. Around Antarctica, where most of the ice does not survive the summer melt, brine drainage is the most important method of sea-ice desalinization. The effects of ice salinity on electromagnetic radiation will be discussed later.

Sea-ice cover in the polar regions is not a continuous mass of ice. Wind, waves, currents, and internal stresses constantly act on the ice resulting in deformation and fractures. Open water that occurs in the ice pack includes leads and polynyas. Leads are linear openings in the ice pack whereas polynyas are nonlinear, irregularly-shaped openings. Polynyas will be discussed in greater detail later in the text. Fracturing of the ice pack produces large, irregularly-shaped sections of ice called floes. Ice floes often collide and can form ridges and keels or can raft. Ridges and keels result when the floes are compressed with

enough force to crumble the ice into piles on top of the ice or to force the ice below sea level. Rafting occurs when one floe overrides another. Ice floes range in size from tens of meters to as large as 10 km, yet detection of individual floes via satellite observation depends on the type of sensor used [*Stringer*, 1984].

Remote Sensors and Radiation Principles

Remote Sensors

The physical setting and conditions around Antarctica make large-scale *in situ* observations nearly impossible. At its maximum extent, sea ice covers about 20 million square kilometers of the Southern Ocean. Shipboard and aircraft observations of the ice are spatially limited and, therefore, impractical. In addition, the climate of the polar regions is dominated by harsh winds and cold temperatures which make surface observations hazardous and uncomfortable. Expeditions to the waters around Antarctica are also very expensive and any data collected from these expeditions are of limited scientific value due to the limitations of time and space. *In situ* measurements are, however, very important for substantiating the assumptions made in the applications of remote sensing. Remote sensing offers a practical, inexpensive, large-scale view of the polar regions.

The atmosphere is a complex medium of gasses, liquids, and suspended particles that can absorb and/or scatter

radiation. The extent of the atmospheric attenuation depends on the wavelength of radiation, the size of the suspended particles or liquids, and the chemical properties of the gasses and liquids. Certain wavelengths of radiation are not attenuated by atmospheric effects. Figure 1 illustrates those wavelengths which have high transmission characteristics. In order to avoid extensive attenuation, remote sensing observations must be made in regions of high atmospheric transmission. Sensors that utilize these atmospheric "windows" are divided into 5 categories, determined by their respective wavelength of operation: visible (VIS), infrared (IR), passive microwave (PMW), active microwave (AMW), and radar altimeters.

_ VIS sensors measure the amount of light that has been reflected by the surface and are useful in detecting snow and ice which have high albedos. However, VIS sensors are useless at night and during periods of cloud cover when there is little or no light to be reflected from the surface. IR sensors are able to detect temperature differences between objects and are also useful in monitoring ice edge location. However, IR radiation cannot penetrate cloud cover either. VIS and IR sensors cannot monitor the polar regions on a continuous, long-term basis because they are limited by cloud cover and one-half year of darkness annually and are therefore not practical for remotely sensing sea ice on a continuous basis.
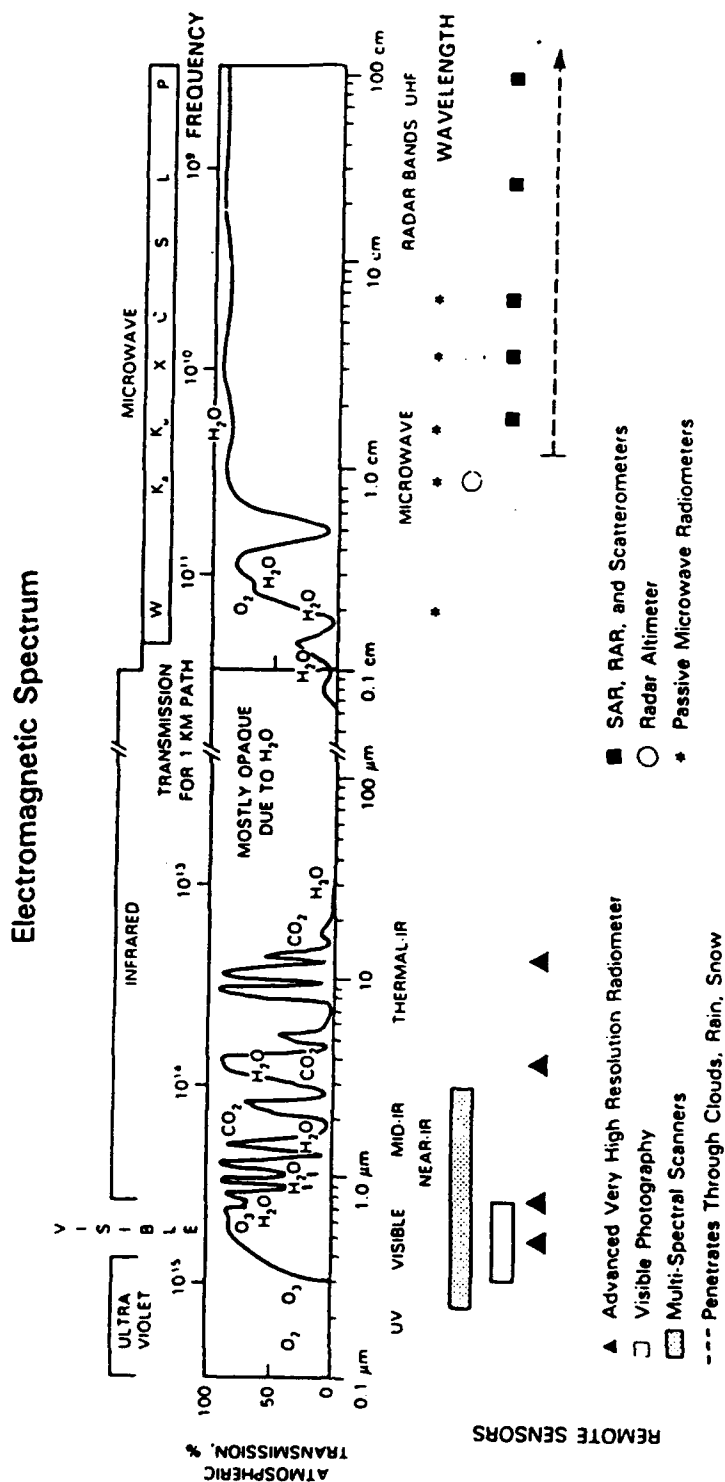
Figure 1. Electromagnetic spectrum from ultra-violet to microwave wavelengths. Atmospheric windows are indicated in the white regions and location of various satellite sensor channel locations are shown by their respective symbols [after Comiso, 1991].

Radar altimeters, on the other hand, are day/night and almost all-weather capable. They measure the distance from the surface to the satellite to produce a measurement of surface elevation. Their resolution is fine enough to distinguish the elevations of ice and the ocean. However, radar altimeters have a narrow field of view (FOV) and are impractical for large-scale observations. They also do not produce imagery and cannot derive ice concentration.

Microwave radiation, in the range 1-200 GHz, is insensitive to atmospheric effects and is only affected by precipitation at higher frequencies (>90 GHz) [Massom, 1989]. AMW systems transmit a signal and measure the radiation reflected or scattered back to the receiver from the surface while PMW systems measure the naturally emitted radiation from the surface. AMW sensors have a resolution on the order of 10 m; however, they have a narrow FOV and are suited more for regional rather than global studies. PMW systems have a considerably poorer resolution, or instantaneous field of view (IFOV), but have a large FOV which make them the most practical sensor for large-scale observations.

The poor resolution of PMW sensors may seem like a disadvantage but it actually makes PMW sensors more capable in determining ice concentration. PMW systems use an integrating technique to analyze data rather than the resolving technique used by higher-resolution systems [Parkinson et al., 1987]. Ice floes and open-water features within the ice pack are often the same size as or smaller

than the resolution of radar, VIS, and IR imagery. These
sensors cannot resolve polynyas or leads and, therefore,
cannot determine the ice concentration within the IFOV of the
satellite [Parkinson et al., 1987]. The integrating
technique integrates the emission from both open water and
ice within the IFOV. Because of the significant difference
in emissivities of water and ice, approximate values of
concentrations are determined by interpolation from the
integrated emission [Parkinson et al., 1987].

Microwave Radiation Principles

Passive microwave sensors measure the thermally emitted
radiation from the earth's surface. The black body curves of
Figure 2 illustrate the wavelengths of maximum emission from
the earth. The microwave region, located far off the right
side of the graph, accounts for very little of the earth's
overall emission. This emission is small enough to be
proportional to the first power of temperature while the
majority of the spectrum is proportional to the fourth power
of temperature [Stringer, 1984]. This proportionality is
expressed as the Rayleigh-Jean's approximation of Planck's
Law and is written as:

$$T_B = \varepsilon\, T \tag{1}$$
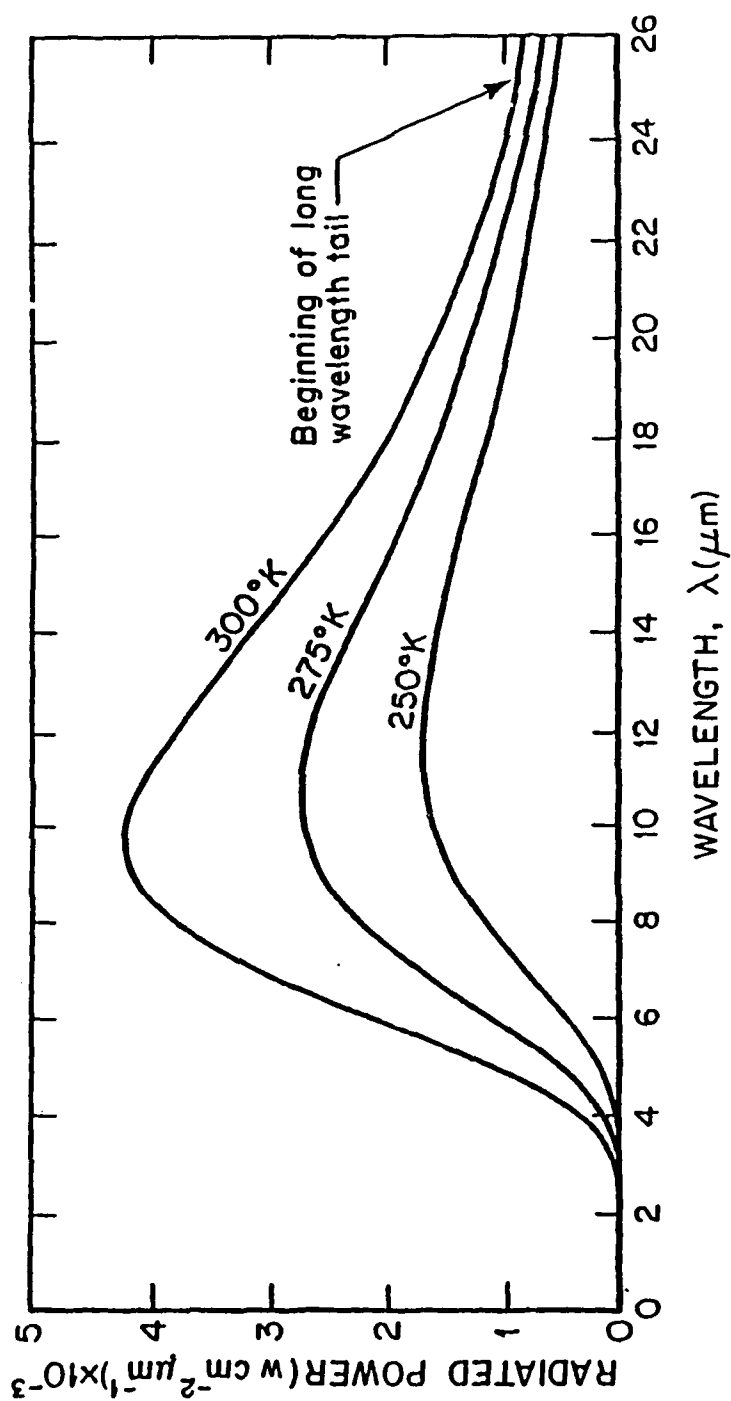
Figure 2. Blackbody Curves for the Earth as a function of wavelength and temperature [after Stringer, 1984].

where T_B is the brightness temperature, or emittance, T is the emittor's physical temperature, and ε is the emissivity of the emitter. The Rayleigh-Jean's approximation assumes that the radiating material is non-scattering, homogeneous, and isothermal [Massom, 1989]. This obviously will lead to some error in dealing with sea ice; however, the error is overlooked for simplicity.

Emissivity is the ratio of radiant flux emitted by a material to that emitted by a black body at the same temperature [Massom, 1989]. Emissivity is a characteristic unique to each emitter as it is highly dependent on the physical composition and structure of the material. Figure 3
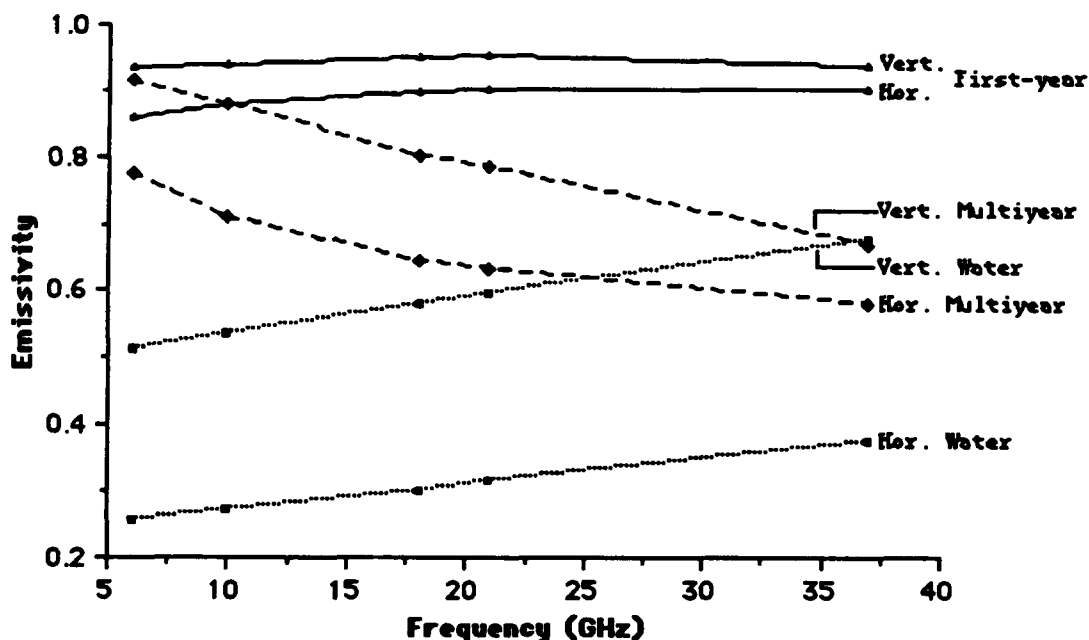
Figure 3. Emissivities for water, first-year ice, and multiyear ice measured during NORSEX-79 [NORSEX Group, 1982].

demonstrates the variance of emissivity observed during the NORSEX-79 experiment with respect to surface type, frequency, and polarization. Obvious differences in the emissivities of water, first-year ice and multiyear ice can be exploited by a microwave sensor. The contrast between ice and water arises from the high albedo of ice as opposed to the lower albedo of water.

Parkinson et al. [1987] attributes most of the difference between ice types to the brine contained in the freeboard layer of the ice. Figure 4 illustrates the parameters that influence the emissivity of first-year and multiyear ice. Emissivity generally increases with increased salinity within the ice. In first-year ice, most of the brine incorporated into the ice structure during formation has not had an opportunity to drain, leaving a high salinity. Hence, first-year ice has the higher emissivity. Multiyear ice, however, has undergone brine drainage during the summer melt season and has a considerably lower salinity and, accordingly, emissivity.

Another important parameter affecting emissivity is the amount of scattering induced by the ice. As seen in Figure 4, first-year ice has a relatively smooth surface which will increase the amount of radiation reflected to space. Multiyear ice, on the other hand, has a rough surface as a result of the melt season and also many internal air pockets left from the brine drainage. These two features scatter
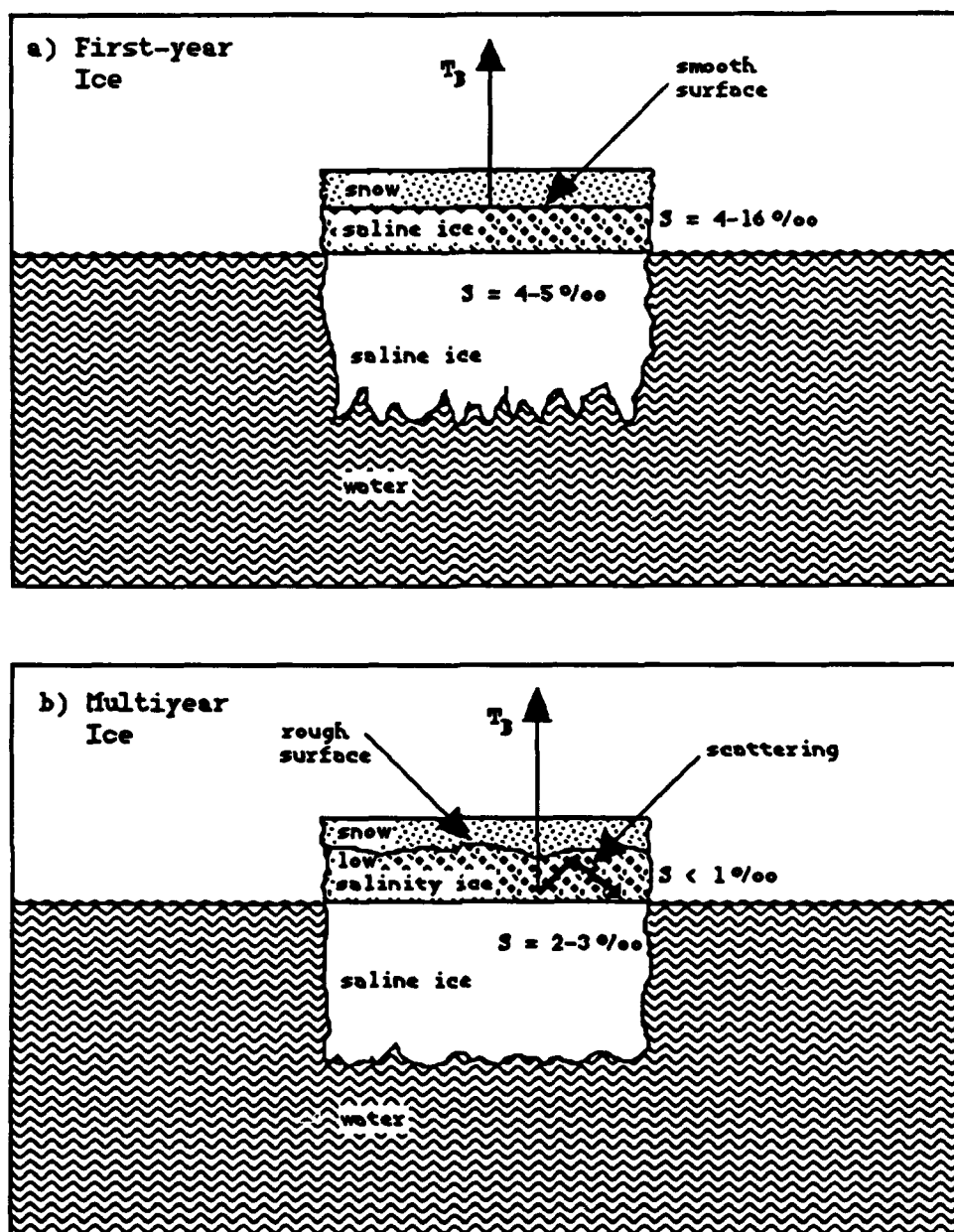
Figure 4. Schematic Diagram of the Microwave Properties of Sea Ice [after Parkinson et al., 1987].

radiation that would normally be reflected, further reducing the emissivity.

Microwave energy can be measured at different wavelengths, or frequencies, and at different polarizations

with various trade-offs between the possibilities. Microwave radiation occurs in the frequency range of 1-200 GHz. The higher end of the frequency spectrum offers the best IFOV for satellites. The 85.5 GHz channels of the Special Sensor Microwave/Imager (SSM/I) offer a pixel size of 16x14 km [*NSIDC*, 1990]. However, higher frequencies are scattered by rain and snow because their wavelength approaches the size of the precipitation [*Massom*, 1989]. Low frequencies (6 and 10 GHz) penetrate precipitation and clouds because their wavelengths are large enough to resist scattering. These frequencies, though, provide a much larger IFOV - the 6 GHz channel has a pixel size of 136x89 km [*Robinson*, 1985]. This project utilizes the 19 and 37 GHz channels for each algorithm in order to minimize the size of the data element while limiting atmospheric effects.

Microwave radiation can also be measured at different polarizations. Polarization refers to the plane in which the electrical field oscillates [*Massom*, 1989]. The polarization principle is useful in that materials react differently under vertical and horizontal polarization. In the case of sea ice, vertical polarizations are used because snow cover on top of the ice is believed to adversely affect horizontally polarized radiation [*Svendsen et al.*, 1983].

The atmosphere between the emitting surface and the receiving satellite is a complex medium that affects the received microwave radiation by the satellite. The radiative

transfer equation quantifies these contributions in the following equation:

$$T_B = \varepsilon \ T_0 \ e^{-\tau} + T_1 + (1-\varepsilon) \ T_2 \ e^{-\tau} + (1-\varepsilon) \ T_{sp} \ e^{-\tau} \qquad (2)$$

where T_0 is the surface temperature, τ is the total atmospheric opacity, T_1 is the upward emitted radiance of the atmosphere, T_2 is the downward emitted radiance from the atmosphere reflected back by the surface, and T_{sp} is the radiation from space that enters the atmosphere and is reflected back [Carsey and Zwally, 1986]. In the polar regions, the opacity is small enough that Equation 2 can be rewritten

$$T_B = \varepsilon \ T_0 + \tau \ [(1+k) \ T_a - \varepsilon(kT_a + T_0)] + (1-\varepsilon) \ T_{sp} \qquad (3)$$

with T_a representing the atmospheric temperature and k estimating the diffusiveness of the surface reflection and the vertical distribution of absorption [Carsey and Zwally, 1986]. These equations model the atmospheric contributions received by the radiometer onboard a satellite and are used in the NORSEX algorithm to calculate sea-ice concentration as will be discussed later.

Table 1. Types of sensors and applications [after *Comiso*, 1991].

Visible (0.3 μm < λ < 0.7 μm)
Strength: high resolution
Weakness: darkness and cloud cover
Field of View: 30 m for Thematic mapper, 1 km for Advanced
    Very-High Resolution Radiometer (AVHRR), 10 m for SPOT
Applications: ice edge, ice thickness, chlorophyll
    concentration, primary production, snow mapping, cloud
    cover, albedo

Infrared (0.7 μm < λ < 13 μm)
Strengths: night/day, good resolution
Weakness: cloud cover
Field of View: 1 km for AVHRR, 6 km for THIR
Applications: surface temperature, cloud cover, snow, water
    vapor, storm tracking, ocean current tracer, humidity
    profile

Passive Microwave (1 mm < λ < 1 m)
Strengths: night/day, almost all weather, global coverage
Weakness: poor resolution
Field of View: 25 to 150 km
Applications: ice concentration, ice edge, atmospheric water
    vapor, rainfall and wind speed in open ocean, ice and
    sea surface temperature, age of ice, ice extent and area

Active Microwave (1 mm < λ < 1 m)
Strengths: night/day, almost all weather, good resolution
Weaknesses: limited coverage, expensive to process
Field of View: 25 km for Synthetic Aperture Radar (SAR), 1 km
    for altimeter
Applications: ice concentration, ice edge, ice type, ice
    dynamics, ridge/lead statistics, wave penetration, ocean
    current

Radar Altimeter (1 mm < λ < 1 m)
Strengths: night/day, almost all weather, good resolution
Weakness: non-imaging
Vertical Range Accuracy: 10 cm
Applications: topography, ice-edge identification

Passive Microwave Sensors

History of Passive Microwave Remote Sensing

Passive microwave (PMW) sensors have their origins in the early 1960's. In 1962, Mariner 2 used a PMW radiometer to observe the surface of Venus [Massom, 1989]. The Soviets then used PMW radiometers on Cosmos 243 and Cosmos 384 in 1968 and 1970, respectively. These sensors were used for remote sensing of the earth's surface as were subsequent satellites from the Intercosmos, Cosmos, and Meteor series [Massom, 1989]. Large-scale observations of the polar ice · coverage were not available, though, until the launch of the Nimbus 5 satellite in December 1972. This satellite carried the Electrically Scanning Microwave Radiometer (ESMR) which detected horizontally polarized radiation at 19.35 GHz. This satellite remained in operation for 11 years but due to degradation of the system, high quality data were limited to the years 1972 to 1976 [Hall, 1985]. In 1975, the Nimbus 6 ESMR satellite was launched and operated at 37.0 GHz receiving both horizontally and vertically polarized radiation.

The different frequency of the Nimbus 6 system allowed for the first multispectral studies of ice and snow cover when analyzed in conjunction with the 19.35 GHz Nimbus 5 data [Hall, 1985]. Multispectral analysis utilizes different frequencies of radiation to analyze the same medium. The

Table 2. Summary of passive microwave space systems.

Sensor	Satellite	Channels	Operational
ESMR-5	Nimbus-5	19 H GHz	12/72 - 06/77
ESMR-6	Nimbus-6	37 H & V GHz	07/75 - 06/76
SMMR	Nimbus-7	37 H & V GHz 21 H & V GHz 18 H & V GHz 10 H & V GHz 6 H & V GHz	10/78 - 08/87
SSM/I	DMSP	85 H & V GHz 37 H & V GHz 22 V GHz 19 H & V GHz	07/87 - Present

behavior of each frequency varies through different types of media and multispectral analysis exploits this variation to differentiate these media and calculate ice concentrations. The advantages of multispectral analysis created the need for a new sensor design that would allow for simultaneous observations from different frequencies.

Scanning Multichannel Microwave Radiometer (SMMR)

The ESMR sensors were phased out in 1978 with the launch of the Nimbus 7 satellite carrying the Scanning Multichannel Microwave Radiometer (SMMR). This system was a ten channel instrument recording data from horizontally and vertically polarized radiation at 37.0, 21.0, 18.0, 10.69, and 6.6 GHz [*Massom*, 1989]. The Nimbus 7 provided instantaneous

multispectral brightness temperature data for a span of
nearly 10 years. Many advances were made in the ability to
differentiate ice types and calculate ice concentrations
during that time span due to the capability of the SMMR
sensor. When data transmission ceased in August 1987, the
SMMR onboard Nimbus 7 had already been replaced by the
Special Sensor Microwave/Imager (SSM/I) on the Defense
Meteorological Satellite Program (DMSP) satellite.

Special Sensor Microwave/Imager (SSM/I)

With the Nimbus 7 having already exceeded its predicted
lifetime, the NASA Polar Oceans Program established a Science
Working Group (SWG) to create a program to augment the
extensive database initiated by the ESMR and SMMR sensors
[*Weaver*, 1987]. The SWG decided the goals of the SSM/I
should be twofold: 1) extend the database of ice extent and
concentration in order to monitor the variability and trends
of sea ice and 2) improve the understanding of ice-ocean-
atmosphere interactions by studying various aspects of the
ice pack [*Weaver*, 1987]. These aspects would include snow
cover, surface albedo, surface roughness, ice and current
velocities, and the temperatures of the ocean, ice, and
atmosphere. The SSM/I was designed and built by Hughes
Aircraft to the specifications listed in Table 3. The DMSP
F8 satellite carrying the SSM/I sensor was launched on 20
June 1987 into a near-polar, sun-synchronous orbit [*Weaver*,

1987]. Data transmission began on 8 July 1987 [*National Snow and Ice Data Center*, 1990]. The Navy's Fleet Numerical Oceanography Center (FNOC) receives and processes the data and then passes the data on to the National Snow and Ice Data Center (NSIDC) for archiving and distribution [*Weaver*, 1987]. The SSM/I sensor has conducted daily observations of the polar regions since its launch with the exception of one period from 3 December 1987 to 12 January 1988. The sensor was shut down at this time due to excessive heating of the instrument by solar radiation [*NSIDC*, 1990].

Table 3. SSM/I performance characteristics.

Center Frequency, GHz	19.35	22.24	37.00	85.5
Polarization	H & V	V only	H & V	H & V
Effective FOV, km	70x45	60x40	38x30	16x14
Brightness Resolution, °K	0.8	0.8	0.8	0.8
Swath Width, km	1349	1349	1349	1349

Algorithms

The satellite sensor receives brightness temperature and then transmits these data back to earth. These data are then archived, copied to compact discs, and made available for distribution. Complex algorithms exist that use the previously discussed radiative, atmospheric, and surface

characteristics to derive sea-ice concentrations from these brightness temperatures.

NORSEX Algorithm

Of the three algorithms considered in this research, only the NORSEX algorithm attempts a theoretical approach to the analysis of the satellite data. The algorithm applies theories of radiation physics with a model of the surface and a model of the atmosphere. These models are based on data and characteristics observed in the Arctic region and, therefore, lend themselves to some degree of error when applied to the Antarctic.

Microwave radiation is emitted and reflected from somewhere between the surface and the bottom of a sheet of sea ice and also from the surface of the ocean [*Svendsen et al.*, 1983]. The surface model attempts to quantify the amount of emitted radiation from the combined ice-water surface. As discussed previously, the amount of radiation received by a radiometer immediately above the surface, called the emitted brightness, is represented by the Rayleigh-Jean's approximation of Planck's law (Equation (1)). The surface is treated as a conglomeration of open water, first-year ice, and multiyear ice so that their respective concentrations (C_w, C_f, and C_m) sum in the following manner:

$$1 = C_w + C_f + C_m. \tag{4}$$

Svendsen et al. [1983] expanded Equation (1) to include the different components of the surface and their contributions:

$$T_E = C_w \mathcal{E}_w T_w + C_f \mathcal{E}_f T_{ice} + C_m \mathcal{E}_m T_{ice}. \qquad (5)$$

The emissivities, $\mathcal{E}_w$, $\mathcal{E}_f$, and $\mathcal{E}_m$, have been measured by shipborne radiometer during the NORSEX experiment and are recorded in Table 4 [Svendsen et al., 1983]. The temperature

Table 4. Emissivities measured during the NORSEX-79 experiment [Svendsen et al., 1983].

	19V GHz	37V GHz
Water	0.621	0.712
First-year ice	0.950	0.950
Multiyear ice	0.800	0.650

of the water, T_w, is easily measured and is set to 272° K for these calculations [Svendsen et al., 1983]. The temperature of the ice, however, is not easily measured. The temperature of the ice will fall between the atmospheric temperature, T_a, and the oceanic temperature due to the temperature gradient between the two. The ice temperature is a function of these two quantities and is expressed as:

$$T_{ice} = \alpha T_a + (1 - \alpha)T_w \qquad (6)$$

[*Svendsen et al.*, 1983]. The coefficient α was estimated by means of studies of the variation in T_E with respect to T_a off Ellesmere Island and is given the value 0.4 (Svendsen et al. 1983). Equations (4)-(6) represent the surface model of the NORSEX algorithm.

The atmospheric temperatures, which vary significantly throughout the year, directly affect the temperature gradient across the ocean-atmosphere interface and, therefore, the amount of ice present. The NORSEX group developed the algorithm to deal with Arctic conditions and used 270° K and 250° K for the atmospheric temperature in the Subarctic and Arctic, respectively [*Svendsen et al.*, 1983]. To adapt the algorithm for use in the Antarctic and to improve its accuracy, average monthly surface temperatures were used as input to the algorithm in this project. The temperatures were taken from the Joint U.S. Navy/U.S. Air Force Climatic Study of the Upper Atmosphere and the criteria for selection consisted of temperatures at 1000 mb around 65° S in the Weddell Sea [*National Climatic Data Center*, 1989]. The temperatures used for the algorithm are listed in Table 5.

The second portion of the NORSEX algorithm is an atmospheric radiation model. The radiation received by the satellite, T_H, originates from four different sources (see Figure 5): (1) emitted radiation from the earth's surface,

Table 5. Mean monthly atmospheric surface temperatures
in the Weddell Sea at 1000mb and 65° S [NCDC, 1989].

Month	Temperature (°K)
January	273.0
February	271.5
March	270.5
April	265.5
May	263.0
June	260.5
July	258.0
August	258.0
September	260.5
October	265.0
November	268.0
December	271.0
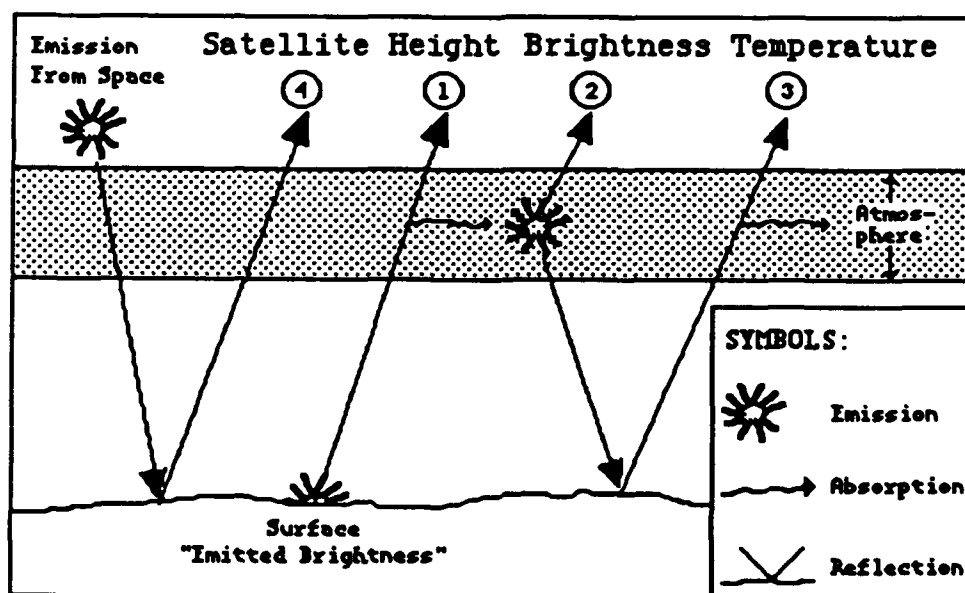
Figure 5. Illustration of the four terms in the
radiation model [after Svendsen et al., 1983].

(2) upwelling radiation from the atmosphere, (3) downwelling radiation from the atmosphere reflected by the surface, and (4) radiation from space reflected by the surface [*Svendsen et al.*, 1983]. This quantity is expressed mathematically as:

$$T_H = \varepsilon_{eff}T_{eff}(1-\tau_a) + \delta T_a\tau_a + (1-\varepsilon_{eff})\delta T_a\tau_a(1-\tau_a) + (1-\varepsilon_{eff})T_{sp} \quad (7)$$
$$\quad\quad\quad (1) \quad\quad\quad\quad (2) \quad\quad\quad\quad\quad (3) \quad\quad\quad\quad\quad\quad (4)$$

where τ_a is the atmospheric opacity and T_{sp} is the temperature of free space, approximately 2.7° K [*Svendsen et al.*, 1983]. Table 6 lists the atmospheric opacities used in the calculations. By substituting T_E for $\varepsilon_{eff}T_{eff}$, T_E can be calculated from T_H by

$$T_E = (T_H - 2\delta T_a\tau_a + \delta T_a\tau_a^2 - T_{sp})/$$
$$[1-\tau_a - \beta\delta(\tau_a-\tau_a^2) - \beta(T_{sp}/T_a)]. \quad (8)$$

Table 6. Atmospheric opacities for the Arctic and Subarctic atmospheres [*Svendsen et al.*, 1983].

	19V GHz	37V GHz
Arctic	0.03	0.07
Subarctic	0.04	0.10

The constants β and δ are given values of 0.95 and 0.9 for the purpose of calculation [*Svendsen et al.*, 1983]. Equation (8) is the practical representation of the atmospheric model (Equation (7)) used to calculate the ice concentrations.

The algorithm will calculate the values for first-year and multiyear ice concentrations. In the Southern Ocean, however, there is very little ice that survives the melt season and becomes multiyear ice. The NASA Team and Comiso algorithms calculate the total concentration of sea ice, not the fractional concentrations of individual ice types. In order to compare the total concentrations predicted by each algorithm, the first-year and multiyear values are added in the NORSEX algorithm to get the total concentration. The algorithm begins with the input of data from the two chosen satellite channels. The algorithm consists of the following steps [*Svendsen et al.*, 1983]:

1. The satellite data are calibrated to give the proper brightness temperatures at satellite height.

2. The emitted brightness is calculated based on the assumption of atmospheric temperature over 100% ice.

3. By solving Equations (4), (5), and (8) simultaneously (two channels gives two equations with two unknowns), the initial ice concentrations are found.

4. A refined atmospheric temperature is found by using the total ice concentration calculated in step 3 to linearly interpolate between the surface temperature over open water and over 100% ice.

5. Steps 2 and 3 are repeated using the refined
atmospheric temperature to get a refined total ice
concentration.

Comiso Algorithm

The Comiso algorithm exploits the differences in surface
emissivities to solve for ice concentration using a bootstrap
technique [Comiso, 1991]. Comiso attempts a more
engineering-oriented approach because he feels that radiative
transfer models of sea ice, as in the NASA Team and NORSEX
algorithms, have not accurately taken parameters such as
brine volume, ice wetness, and grain size into account
[Comiso, 1991]. Comiso's algorithm is based on the use of
scatter plots, shown in Figure 6. Three-dimensional plots
like Figure 6a display emissivities from three frequencies
(10, 18, and 37 GHz) and help investigate the vertical
structure of sea ice as optical depth is dependent on
wavelength [Comiso and Sullivan, 1986]. Polarization plots
like Figure 6b differentiate surface types due to the
dependence of polarization characteristics on surface type
[Comiso and Sullivan, 1986]. Figure 7 shows two-dimensional
frequency and polarization plots of brightness temperature
data from the Weddell Sea region. The theory behind these
scatter plots postulates that clusters of data correspond to
different surface types. Comiso and Sullivan [1986] have
found that data along line AB correspond to consolidated,
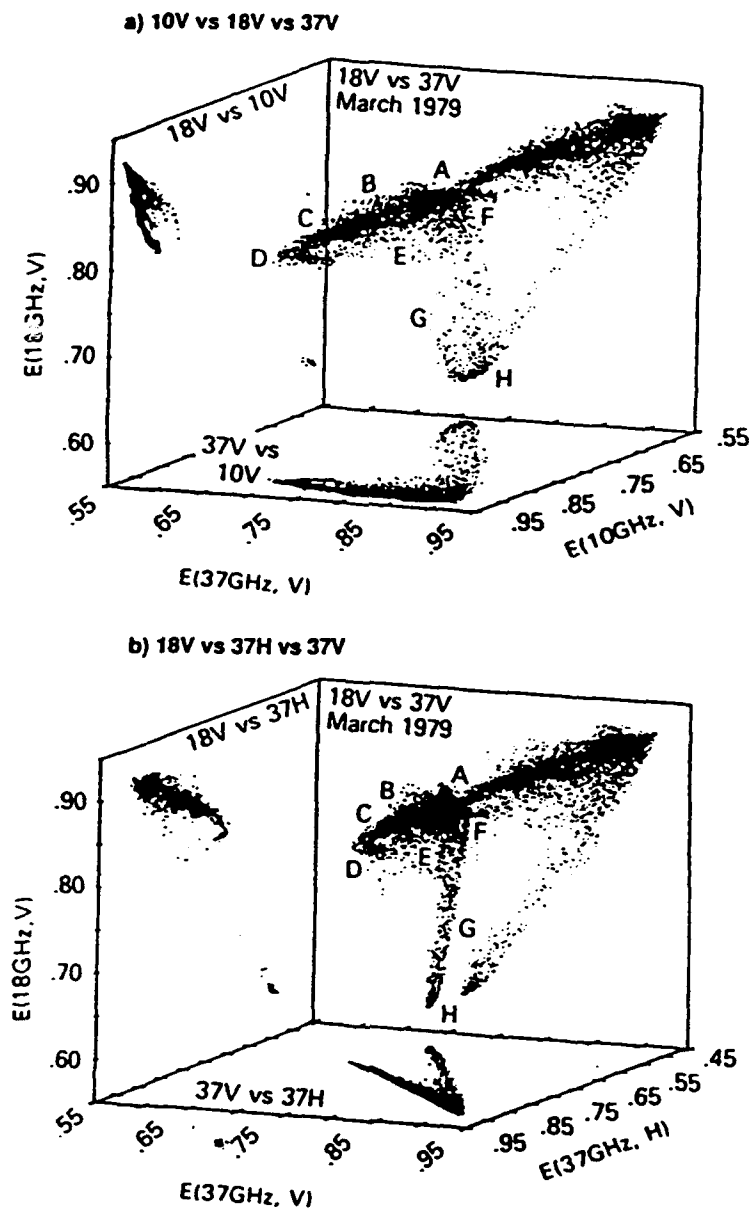
Figure 6. Three-dimensional emissivity scatter plots for (a) 37V vs. 18V vs. 10V and (b) 18V vs. 37H vs. 37V [after *Comiso*, 1991].
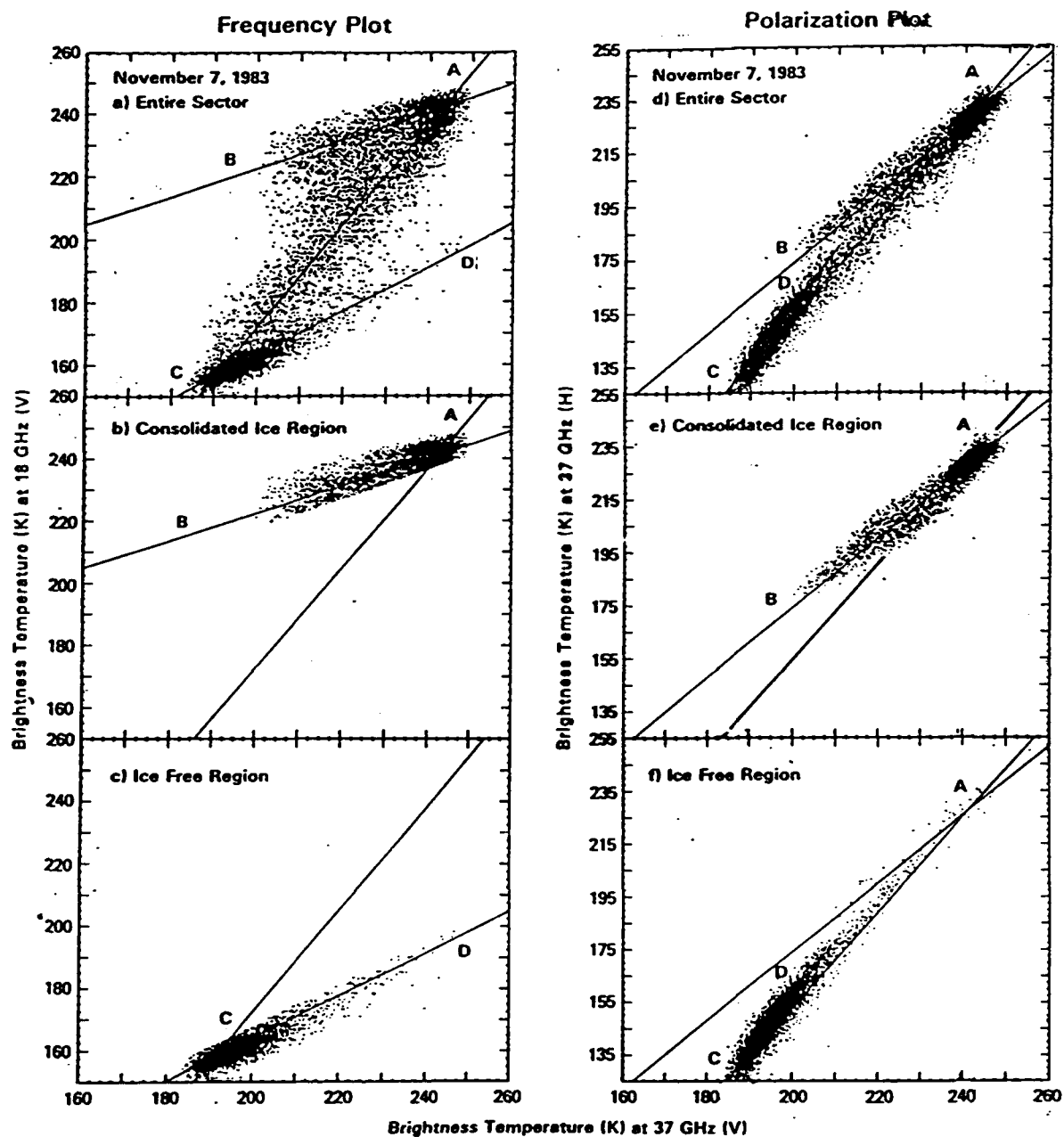
Figure 7. Frequency and Polarization brightness temperature scatter plots [after *Comiso and Sullivan*, 1986].

100% ice; line CD represents ice-free ocean; and data
scattered along line AC are a mixture of ice and open water.
In the polarization plot, much of the consolidated ice data
fall along the ice-ocean mixture line and could lead to an
underestimation of 100% ice. Similarly, the open water data
fall along the ice-ocean line and will produce inflated
values of ice concentration. These points indicate that a
frequency plot will be more effective for calculating sea-ice
concentration. The frequency plot, using 19 and 37 GHz,
vertical polarization, was chosen over the polarization plot
because of the aforementioned advantages. These particular
frequencies were chosen to minimize atmospheric attenuation
and maximize resolution as discussed earlier.

The retrieval of ice concentration by the Comiso
algorithm is based upon the ratio of brightness temperatures
given by:

$$C = (T_S - T_W)/(T_I - T_W) \tag{9}$$

where T_S, T_I, and T_W refer to the brightness temperatures of
the given data point, 100% ice, and open water, respectively
[Comiso and Sullivan, 1986]. The technique used to arrive at
an ice concentration is graphically displayed in Figure 8.
For a data point T, the concentration is expressed as a ratio
of the magnitudes of the vectors r_I and r_T, as this ratio
is the same as that expressed in Equation (9). The proper T_I
to use for data point T is given by I and this point is

Figure 8. Schematic diagram illustrating the technique for calculating sea ice concentration [after *Comiso and Sullivan*, 1986].

determined by solving the equations of lines AB and CT simultaneously. The equation for AB is a predetermined input to the algorithm. The slope of AB is set to 0.45 and point A is defined by 262.0° K for 37 GHz and 256.0° K for 19 GHz [*Com*so, 1989]. Line CT is defined by point C, given by 205.0 for 37 GHz and 182.0 for 19 GHz, and by point T, given by the data point location [*Comiso*, 1989]. A threshold line ⌐ ides points of open water. This line has a slope 0.8 and intercept 21.0 [*Comiso*, 1989]. The magnitudes of r_I and r_T are determined by using the distance formula as follows:

$$|\mathbf{r}_I| = [(I_{37} - T_{W37})^2 + (I_{19} - T_{W19})^2]^{0.5} \qquad (10)$$

$$|\mathbf{r}_T| = [(T_{T37} - T_{W37})^2 + (T_{T19} - T_{W19})^2]^{0.5} \qquad (11)$$

where T_T's are the brightness temperatures for the data point, T_W's are the brightness temperatures for ice-free water, and I's are the brightness temperatures for the intercept point, I. Dividing $|\mathbf{r}_T|$ by $|\mathbf{r}_I|$ gives the value for the ice concentration.

NASA Team Algorithm

Prior to the launch of the SSM/I sensor, the NASA Sea-ice Algorithm Working Group (NSIAWG) was tasked with selecting an algorithm to use with the new SSM/I data. The NSIAWG chose to use a non-iterative version of an algorithm presented by Cavalieri et al. (1984) [NSIDC, 1990]. This algorithm uses a much-simplified version of the radiative transfer equation as its foundation. Cavalieri et al. [1984] have determined the second and third terms of Equation 3 to be negligible and ignore their contributions. The emission from space is neglected because the contribution is usually < 1° K [Cavalieri et al., 1984]. The contributions from the atmosphere are neglected because the atmospheric opacity in the polar regions is usually very small. For instance, atmospheric radiative transfer models have shown that a variation of 0.2 cm in the atmospheric water vapor column

would increase the opacity by 0.004 for radiation around 19 GHz [*Cavalieri et al.*, 1984]. *Cavalieri et al.* [1984] determined that this change would cause a 0.5% error in the computed ice concentration. The modified version of the radiative transfer equation is expanded to include the different surface contributions and appears as

$$T_B = T_W (1-C) + T_{FY} C(1-F) + T_{MY} CF \qquad (12)$$

where T_W, T_{FY}, and T_{MY} are the brightness temperatures for water, first-year ice, and multiyear ice, respectively; C is the total ice concentration, and F is multiyear ice fraction [*Cavalieri et al.*, 1984]. This is very similar to Equation (5) used in the NORSEX algorithm as part of the surface model. However, the method in which each equation is used is quite different.

The NASA algorithm uses two radiative properties of sea ice and water to calculate ice concentration. Figure 3 illustrates both of these properties. The first property is the large difference between the emissivities of horizontally and vertically polarized radiation from water. The difference between the polarized radiation of first-year and multiyear ice is not as great as that of water. This characteristic is used to differentiate between water and ice. The second property is the difference of emissivity between first-year and multiyear ice at higher frequencies. This observation is used to differentiate between first-year

and multiyear ice in the algorithm. The use of these principles eliminates the dependence of ice concentration on knowledge of the physical temperature of the emitting substance required by the NORSEX algorithm. The NASA algorithm avoids any errors associated with estimating the temperature of the ice and water being observed.

The first portion of the algorithm uses polarization characteristics to quantify total ice concentration. To utilize the large difference in polarization of water, a polarization ratio is defined as:

$$PR = [T_B(V, f) - T_B(H, f)] / [T_B(V, f) + T_B(H, f)] \qquad (13)$$

with the brightness temperatures expressed as a function of polarization (V or H) and frequency (f) [Cavalieri et al., 1984]. Calculations have shown that the difference between PR for water and ice varies from 0.209 at 6.5 GHz to 0.122 at 37 GHz [Cavalieri et al., 1984]. These differences are significant enough to differentiate between ice and water. First-year and multiyear ice are identified by their respective emissivities. This difference is quantified by the gradient ratio, or slope of the lines in Figure 3, between 19 GHz and 37 GHz. This gradient ratio is written as:

$$GR = [T_B(V, 37) - T_B(V, 19)] / [T_B(V, 37) + T_B(V, 19)] \qquad (14)$$

[*Cavalieri et al.*, 1984]. The algorithm uses both the polarization ratio and the gradient ratio in the calculation of ice concentration.

The total ice concentration is computed by combining Equations (12) and (13) to derive a relationship between the concentration and the polarization ratio. The resulting equation is

$$C = (A_1 + A_2 PR)/(A_3 + A_4 PR) \tag{15}$$

where

$A_1 = T_{WV} - T_{WH}$

$A_2 = -(T_{WV} + T_{WH})$

$A_3 = (T_{WV} - T_{WH}) - (T_{FYV} - T_{FYH})(1-F) - (T_{MYV} - T_{MYH})F$

$A_4 = -(T_{WV} + T_{WH}) + (T_{FYV} + T_{FYH})(1-F) + (T_{MYV} + T_{MYH})F$

Table 7. Measured SSM/I Brightness Temperatures for the Southern Ocean [*NSIDC*, 1990].

Surface Type	Frequency (GHz)	Temperature ($^\circ$K)
Open Water	19V	175.3
	19H	97.7
	37V	199.6
First-year Ice	19V	251.2
	19H	241.7
	37V	248.3
Multiyear Ice	19V	223.2
	19H	203.9
	37V	186.3

[*Cavalieri et al.*, 1984]. The coefficients A_1 to A_4 are functions of the emitted radiances of water (T_W), first-year ice (T_{FY}), and multiyear ice (T_{MY}) for horizontally and vertically polarized radiation at 19 or 37 GHz. These radiances are measured brightness temperatures for each respective medium and are listed in Table 7. This portion of the algorithm exploits the polarization characteristics of a single frequency in order to differentiate between water and ice.

The second half of the algorithm focuses on how much of the ice calculated in Equation (15) is multiyear and how much is first-year ice. To do this, Equations (12) and (14) are combined to give

$$F = (B_1 + B_2GR)/(B_3 + B_4GR) \tag{16}$$

where
$$B_1 = [T_W(37V) - T_W(19V)](1-C) + [T_{FY}(37V) - T_{FY}(19V)]C$$
$$B_2 = -[T_W(37V) + T_W(19V)](1-C) - [T_{FY}(37V) + T_{FY}(19V)]C$$
$$B_3 = [T_{FY}(37V) - T_{FY}(19V)]C - [T_{MY}(37V) - T_{MY}(19V)]C$$
$$B_4 = -[T_{FY}(37V) + T_{FY}(19V)]C + [T_{MY}(37V) + T_{MY}(19V)]C$$

[*Cavalieri et al.*, 1984]. The B coefficients also depend on the same brightness temperatures in Table 7. These equations differentiate between ice types using the variations in the brightness temperatures of the ices caused by their difference in emissivity.

Equations (15) and (16) are interdependent based on the unknowns C and F. *Cavalieri et al.* [1984] eliminate this

interdependence through an iterative process. First, the radiances measured by the satellite are read into the algorithm to calculate PR and GR. Next, the initial ice concentration, C, is calculated using these ratios, the measured brightness temperatures, and an assumption of 50% for the multiyear ice fraction, F [*Cavalieri et al.*, 1984]. After this computation, a new multiyear fraction is calculated with the ice concentration, C, computed in the previous step. An iterative procedure is then followed to derive the final ice concentration and multiyear fraction. The NASA Team modified the Cavalieri et al. algorithm to avoid the iterative process and ease the calculations [*NSIDC*, 1990]. This was done by modifying the coefficients to remove the interdependence.

Application of Algorithms

The data used to run the algorithms was supplied by the National Snow and Ice Data Center (NSIDC) in Boulder, Colorado. NSIDC provided two types of data on compact discs: brightness temperature grids and precalculated ice concentration grids. The ice concentration grids were determined by both the NASA and the Comiso algorithms and covered the time period 9 July 1987 to 31 December 1989. The brightness temperature grids extended the data set another 6 months through 30 June 1990. The NORSEX ice concentration grids were determined using the computer program in Appendix

A for the entire period. In the interests of time and
computer storage, the precalculated ice grids were used for
the NASA and Comiso algorithms with the final 6 months added
using the program in conjunction with the brightness
temperature grids. It was discovered that the ice grids
using the Comiso algorithm from August to December 1988 were
incorrect on the compact discs. To rectify the situation,
these five months were recalculated using the computer
program and the brightness temperature data. In order to
manipulate the large gridded data sets, a subset version of
the MICRODEM program was employed [Guth, 1990].

Certain measures have been taken in order to generate
high-quality, accurate images of sea-ice concentration.
Initial images generated by the three algorithms showed a
great deal of low-concentration sea ice where there should
have been open ocean. The NASA Team algorithm applies the
gradient ratio to filter out the appearance of these low-
concentration pixels that result from atmospheric
contributions such as cloud cover and precipitation [NSIDC,
1990]. A gradient ratio value greater than 0.05 is assumed
to be atmospheric contributions and the ice concentration
value is set to 0 percent. This "weather filter" was applied
in each of the three algorithms and managed to eliminate most
of the false concentrations.

Initial ice concentration images also displayed
significant amounts of missing data. Some of the data
recorded by the satellite fell out of the range of reasonable

expectations and are flagged as bad, or missing, data [*NSIDC*, 1990]. Weekly averages of sea-ice concentration were computed to remove the presence of these bad data. The weekly average proved useful in that it reduced the amount of data to work with and also managed to "smooth" the data. Several days during the three-year period of observation do not contain any data because of various instrument problems. The time average ignores these days and computes the average for a lesser number of days. The time period from 3 December 1987 to 12 January 1988, during which the sensor was shut down due to excessive heating, has been deleted from the data set. This gap in the seasonal ice extent and area cycles was filled by interpolation.

Once the initial images were modified and improved, the sea-ice extent and sea-ice area were calculated. In this project sea-ice extent is defined as the area of ocean at least 8 percent of which is covered with sea ice. Sea-ice area excludes areas of open water within the ice pack and only represents the actual ice coverage. The extent is calculated by summing the number of pixels containing greater than or equal to 8 percent ice concentration and then multiplying that number by the area of each pixel - 625 km^2. The area of the pixels was corrected for latitude distortion using an ellipsoidal polar stereographic projection. The sea-ice area is computed by taking the concentration within each pixel, multiplying by the area of the pixel, and then adding the resultant areas. To remove any remnants of false

concentrations along the periphery of the image, a filter was set up to ignore any values north of 53° S latitude (Comiso, personal communication). The ice pack does not normally extend past this point of reference.

One last modification made to improve the accuracy of the algorithms involved using monthly mean atmospheric temperatures as input to the NORSEX algorithm. The original algorithm did not stipulate that variable temperatures be used. The constant-temperature algorithm produced reasonable values for the sea-ice extent; however, the sea-ice area values were significantly lower than the Comiso and NASA values during the winter. Examination of the images revealed that wintertime concentrations were 5-10% lower in the center of the ice pack. Since the NORSEX algorithm attempts to model the atmosphere, it seemed obvious to use variable temperatures to simulate the atmosphere accurately. Results from sea-ice extent calculations remained relatively constant. In the sea-ice area calculations, though, a significant difference was observed during the winter months. Further discussion of this observation follows later in the text.

Polynyas and Heat Flux Model

Polynyas

The *World Meteorological Organization* [1970] defines a polynya as "any non-linear shaped opening enclosed in ice."

Recurring polynyas appear in the same area every year though size, shape, and duration may vary. Polynyas have significant impacts on the biological and physical phenomena of the polar regions. Polynyas within the ice pack are analogous to oases in the desert. Sunlight that passes through openings in the ice raises the amount of primary production [Stewart, 1989]. The increase in primary production attracts animals from all levels of the food chain to the polynya. Many species, including penguins and seals, depend on the annual recurrence of certain polynyas for their existence [Stewart, 1989]. In the physical sense, polynyas enhance the heat and salt fluxes between the ocean and atmosphere. Gow et al. [1990] found that salt fluxes to the ocean are highest during the initial stages of growth when ice is thinnest and growth rates are fastest. Latent-heat polynyas, as will be discussed later, are areas of rapid, continuous ice formation and, therefore, reject large volumes of salt into the underlying water. This salt influx drives much of the vertical circulation around Antarctica. Polynyas also influence the heat transfer between the ocean and the atmosphere. Sea ice acts as an insulator, reducing the amount of heat released to the atmosphere from the ocean. The heat flux through a polynya may exceed the flux through ice cover by a factor of 10 to 100 times [Zwally et al., 1985]. This difference in the amount of heat lost to the atmosphere could have significant effects on the climate system.

Polynyas are classified on the basis of the type of heat flux that drives and maintains the polynya: sensible-heat and latent-heat polynyas. In sensible-heat polynyas, oceanic heat from below melts existing ice and prevents the formation of new ice as heat passes to the atmosphere (Figure 9a). *Muench* [1990] states that this upward heat transfer may result from vertical mixing or through wind-driven upwelling. Topographical upwelling, another cause of upward heat transfer, is believed to be the cause of the Weddell Sea Polynya. *Gordon and Comiso* [1986] speculate that the Maud Rise, a underwater seamount 3500 m higher than the surrounding terrain, deflects warmer deep water to the surface, melting the ice pack. Satellite observations only detected the Weddell Sea polynya during the winters of 1974 – 1976 and 1980 [*Comiso and Gordon,* 1987]. Reduced concentrations were evident the remaining years during the spring breakup and melt of the ice pack.

Latent-heat, or coastal, polynyas normally form over the continental shelf along the coast in the Southern Ocean. Shelf water is much colder than the open ocean and contains very little sensible heat [*Zwally et al.,* 1985]. The heat lost through coastal polynyas is predominantly latent heat due to the rapid, continuous production of ice. Figure 9b illustrates the mechanisms involved in the maintenance of these polynyas. Strong katabatic winds blowing off the continent push the ice pack away from the coast. The newly-exposed ocean quickly refreezes, releasing the heat generated

by the freezing process. The winds push the new ice away again, maintaining the polynya. As seen in Figure 9b, the formation of ice rejects large amounts of salt into the ocean, creating very dense water. This water slides off the continental shelf and becomes Antarctic Bottom Water.

Because of the poor resolution of passive microwave sensors, most polynyas cannot be readily identified due to their small size. Polynyas normally show up on satellite-derived ice concentration images as areas of reduced concentration. There is uncertainty in determining the composition of the surface within the pixels of reduced concentration. A pixel of 50% concentration could be divided into two continuous domains: open water and consolidated pack ice. On the other hand, the same pixel could be a mixture of small ice floes, new ice, and open water. The situation described in the first case would be considered a polynya. However, the area with a reduced, variable ice concentration will also release a large amount of heat to the atmosphere. Most likely, the pixels are a combination of the two possibilities and can be treated as an area of thin, variable concentration ice cover. A recent study by *Worby and Allison* [1991] has investigated the energy exchange over such a surface composition and their findings are applied to the areas of reduced ice concentration that are of interest in this project.
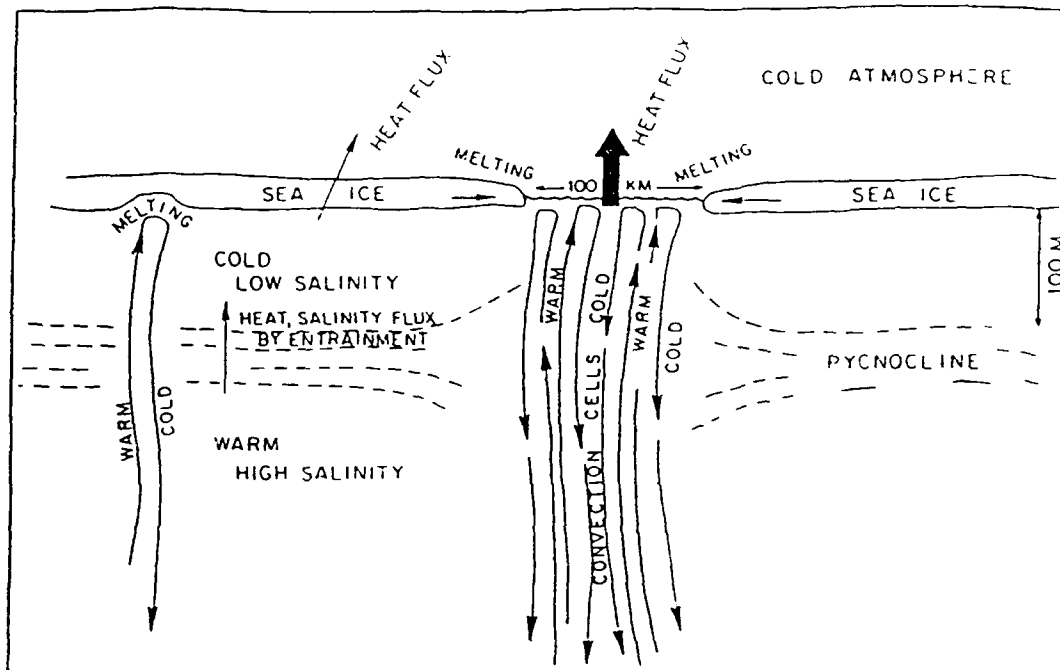
(a)
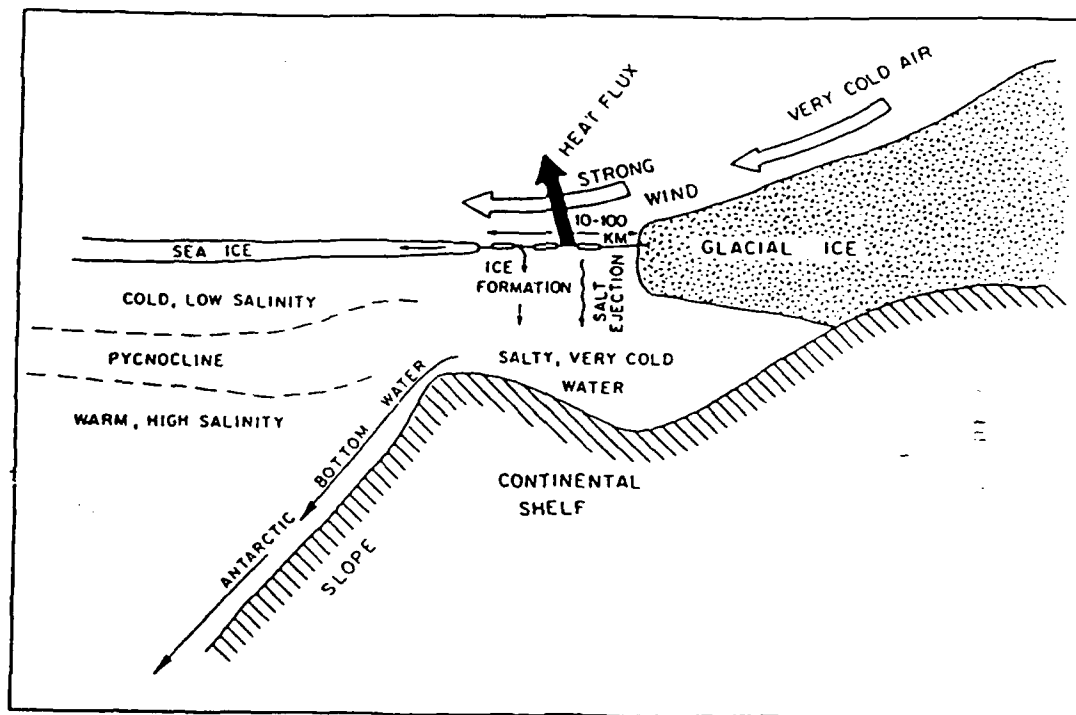
(b)

Figure 9. Models for (a) sensible and (b) latent heat polynyas
[after *Stewart*, 1989].

Energy Exchange Model

The theory behind *Worby and Allison's* [1991] work is that the total energy exchange over a specified area is a summation of the heat lost through the ice and the heat lost from the open water. They quantified the amount of heat lost over varying thicknesses of thin ice around Antarctica and also determined the heat lost through leads and polynyas. To simulate varying conditions of ice concentration, the downwind area under investigation is assumed to be composed of ice floes of constant width (100 m) mixed with leads of variable width [*Worby and Allison*, 1991]. The width of the leads depends on the concentration of ice in the region (Table 8). This width is important to the calculation of turbulent heat loss through leads as discussed later.

Worby and Allison [1991] use an energy budget model developed by *Maykut* [1978] to calculate the energy exchange over thin ice around Antarctica. This model incorporates the

Table 8. Floe and lead dimensions to simulate variable ice concentration [after *Worby and Allison*, 1991].

Ice Concentration (%)	Floe Width (m)	Lead Width (m)
100	100	0
80	100	25
65	100	54
50	100	100
30	100	233

sensible heat flux F_s, the latent heat flux F_e, the conductive heat flux F_c, and the emitted long-wave energy F_1. These parameters are expressed as:

$$F_s = \rho c_p C_s u (T_a - T_o) \tag{17}$$

$$F_e = 0.622 \rho L C_e u (re_{sa} - e_{so}) / p_o \tag{18}$$

$$F_c = [k_o + \beta S_o / (T_o - 273)] (T_b - T_o) / H \tag{19}$$

$$F_1 = \varepsilon \sigma T_o^4. \tag{20}$$

Here, the sensible and latent heat transfer coefficients, C_e and C_s, respectively, are 3.0×10^{-3} and 1.75×10^{-3}, the specific heat of air at constant pressure $c_p = 1004$ J kg^{-1} K^{-1}, the latent heat of fusion $L = 2.8 \times 10^6$ J kg^{-1}, the average air density $\rho = 1.3$ kg m^{-3}, the conductivity of pure ice $k_o = 2.03$ W m^{-1} K^{-1}, σ is the Stefan-Boltzman constant, the long-wave emissivity of the surface $\varepsilon = 0.96$, and the temperature at the bottom of the ice layer $T_b = -1.8°C$ [Worby and Allison, 1991]. The constant β has a value of 0.117 W m^{-1} kg^{-1} [Maykut, 1978]. The remaining variables are unique to conditions in Antarctica: T_o is the surface temperature (K), T_a is the atmospheric temperature (K), u is the wind speed (m s^{-1}), r is the relative humidity (%), e_s is the saturation vapor pressure as a function of T_a, p_o is the atmospheric pressure (kPa), S_o is the salinity of the ice (ppt), and H is the ice thickness (m) [Worby and Allison, 1991]. Worby and Allison [1991] use input values typical of conditions around Antarctica in September for incoming shortwave radiation,

incoming longwave radiation, wind speed, atmospheric
pressure, and relative humidity. The respective heat fluxes
are computed as a function of air temperature and ice
thickness using the aforementioned input.

Worby and Allison [1991] calculated the heat loss over
leads using empirical relationships derived by *Andreas* [1980]
from measurements taken during the AIDJEX Lead Experiment.
The sensible and latent heat losses are functions of the wind
speed, the lead width, the upwind and downwind values of
temperature and specific humidity; the conductivity of air;
and the molecular diffusivity of water [*Worby and Allison*,
1991]. Calculations by *Worby and Allison* [1991] using
variable fetches and air temperatures revealed that the total
turbulent heat flux from a lead is primarily dependent on the
lead width. The relationships used in the calculation of
turbulent heat flux through leads have been verified by *in
situ* measurements by *Andreas and Murphy* [1986] for lead
widths up to 500 m [*Worby and Allison*, 1991].

Comparative Analysis of the Algorithms
Seasonal Sea-ice Analysis

The growth and decay of sea ice around Antarctica
resembles an asymmetric sinusoid in that the pack grows at a
slower rate than it melts. The maximum value normally occurs
in September and the minimum around the end of February. As

discussed earlier, sea-ice coverage may be expressed as an extent or an actual area. Figure 10 shows the sea-ice extent and area calculated in this project. The most obvious characteristic of this cycle is the long period of growth and the rapid rate of ablation. The pack normally grows in size from early March through September - a span of 7 months. The bulk of the decay, however, occurs from late November into early February, not quite 3 months. The monthly growth and decay is shown in Figure 11. These images represent a weekly average from the latter part of each month during 1988. The images were derived from the variable-temperature NORSEX algorithm. The growth can be seen starting in March and lasting through September with no substantial melt occurring until December.

Figure 10a shows the calculated sea-ice extent for each algorithm from 15 July 1987 to 27 June 1990. The minimum and maximum values for extent occur at about the same time for each of the algorithms with the exception of a few anomalies in the cycle. For example, in Figure 10a, the "spike" in the extent given by the Comiso algorithm occurs a month after the maxima from the other algorithms. Overall, the algorithms produce very similar cycles; the difference lies in the amplitude of the cycle. The Comiso algorithm consistently yields the highest values of ice extent with a greater difference in the summer. The increased difference and variation of the Comiso output during summer months is
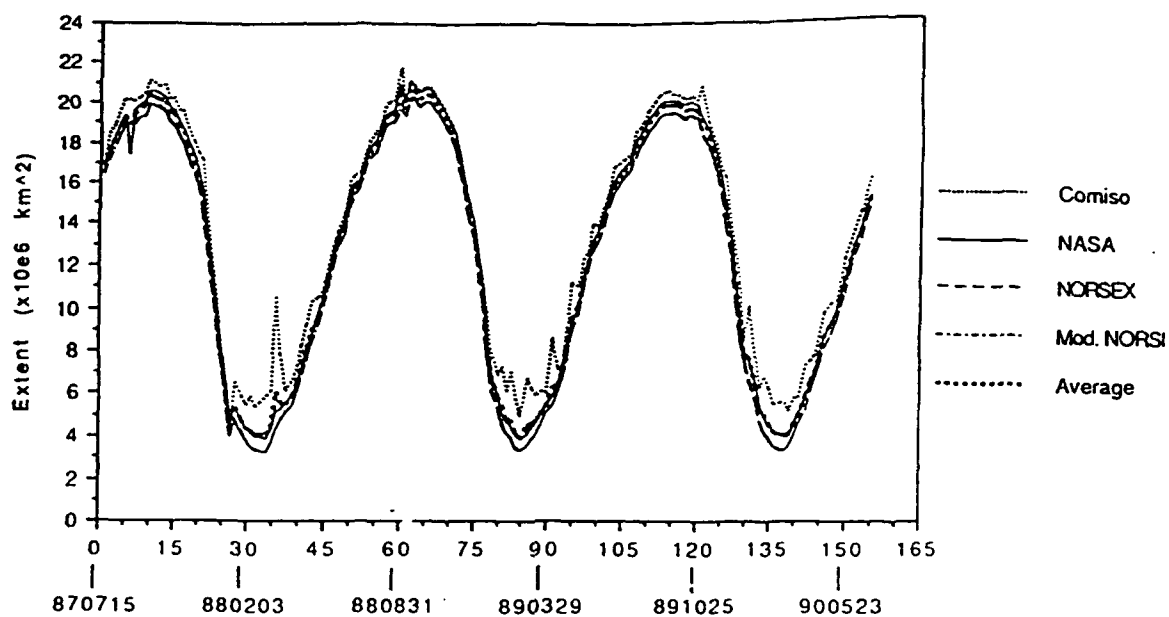
(a)
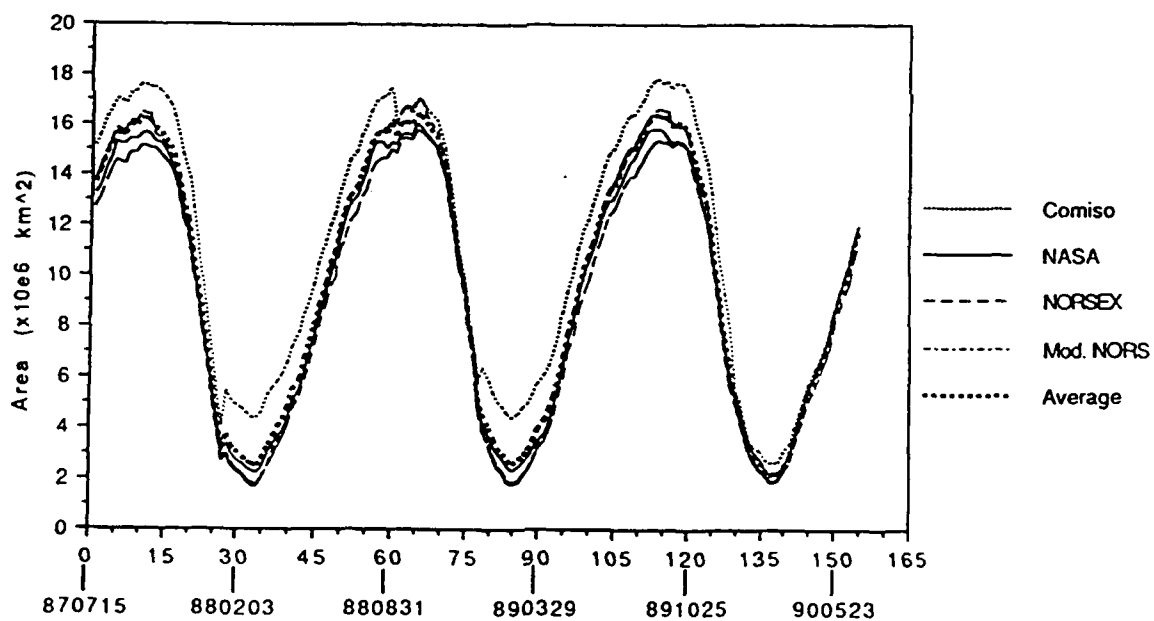
(b)

Figure 10. Seasonal sea ice (a) extent and (b) area cycles calculated in this project.
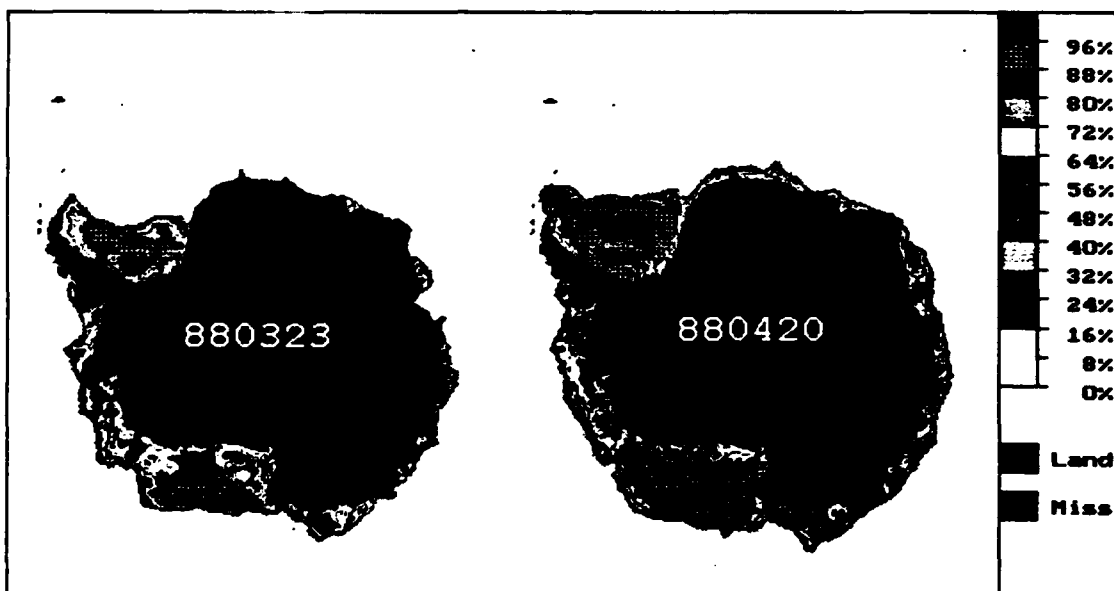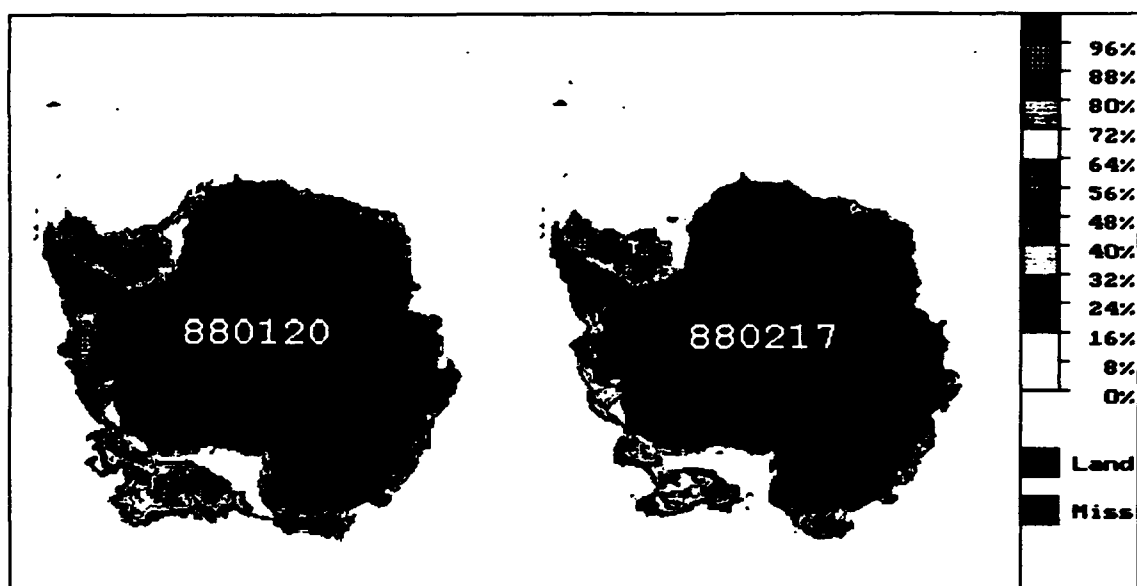
Figure 11a. Averaged weekly ice concentration images
representing January through April 1988 taken from the
variable-temperature NORSEX algorithm.
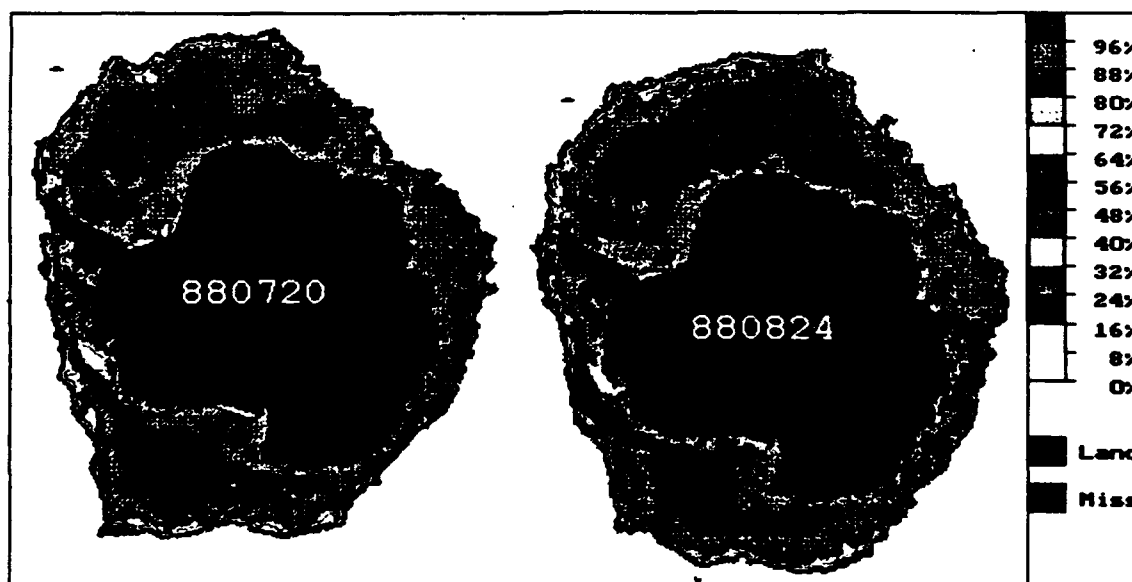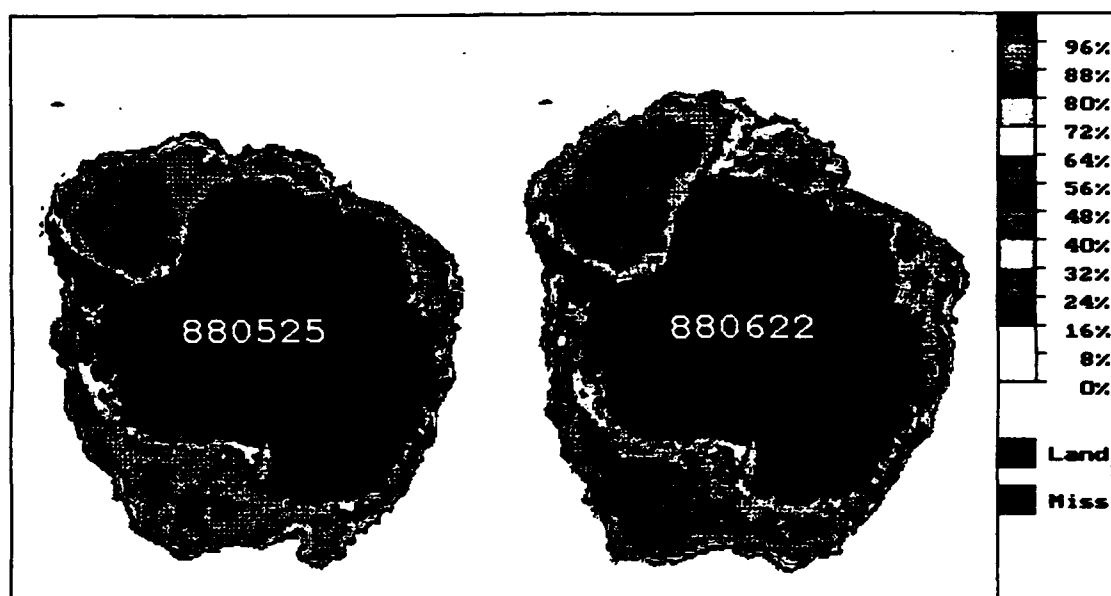
Figure 11b. Averaged weekly ice concentration images representing May through August 1988 taken from the variable-temperature NORSEX algorithm.
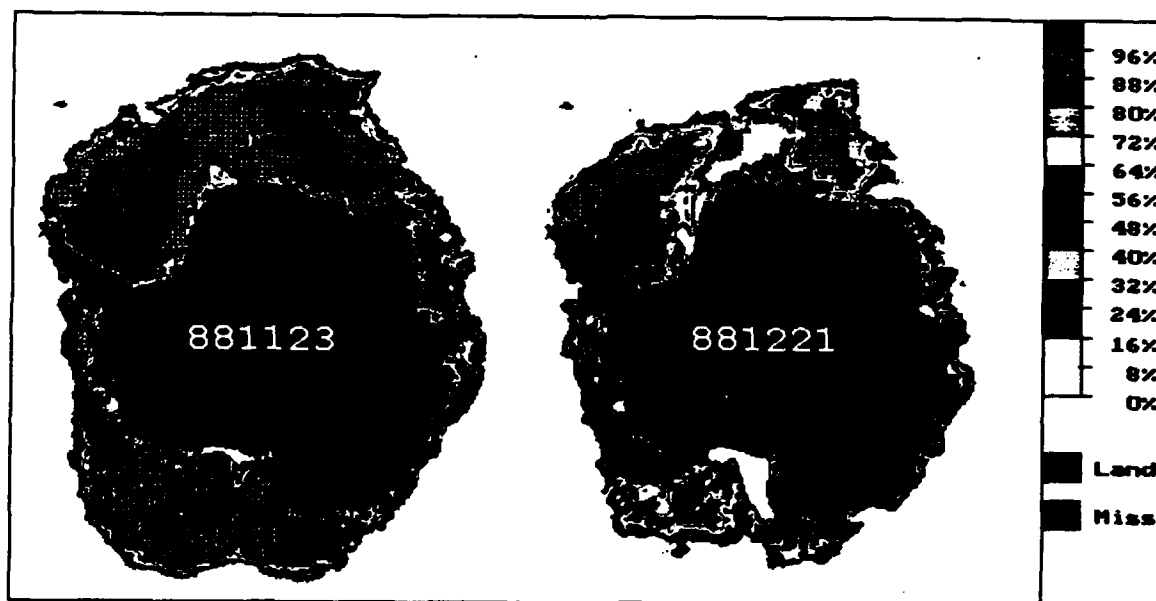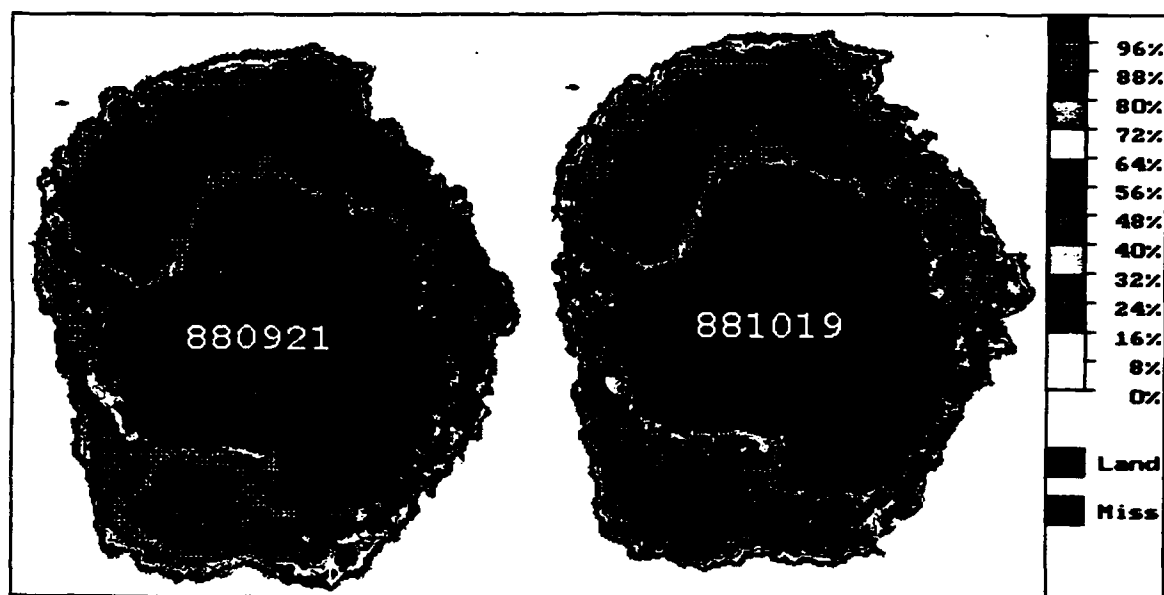
Figure 11c. Averaged weekly ice concentration images representing September through December 1988 taken from the variable-temperature NORSEX algorithm.

attributed to probable false concentrations not eliminated by the weather and latitude filters. The constant- and variable-temperature NORSEX algorithms produce nearly identical results, while the NORSEX algorithm produces values closest to the average of the four algorithms. There does appear to be a slight decrease in the maxima of the cycles but not a corresponding decrease in the minima. Another interesting point regarding Figure 10b is the prediction of the Comiso algorithm when using the brightness temperature grids vice the pre-calculated ice grids. The brightness temperature was used as the input from week 61 to 78 and from 130 to the end. During these periods, the Comiso values are much closer, and even identical at times, to the other algorithms.

The sea-ice areas calculated for each algorithm are shown in Figure 10b. Many of the same characteristics present in the ice extent plot also apply to the area. The Comiso algorithm produces the highest area throughout the year and differences with respect to other algorithms are greater than in the extent analysis. There is not nearly as much weekly variation in the area as compared to the extent plots. Because the pixels that cause the variation in extent have such a low concentration, they contribute very little to the overall ice area. As mentioned earlier, there is a significant difference in the area values generated by the constant- and variable-temperature NORSEX algorithms as displayed in Figure 12. During the summer months, the output
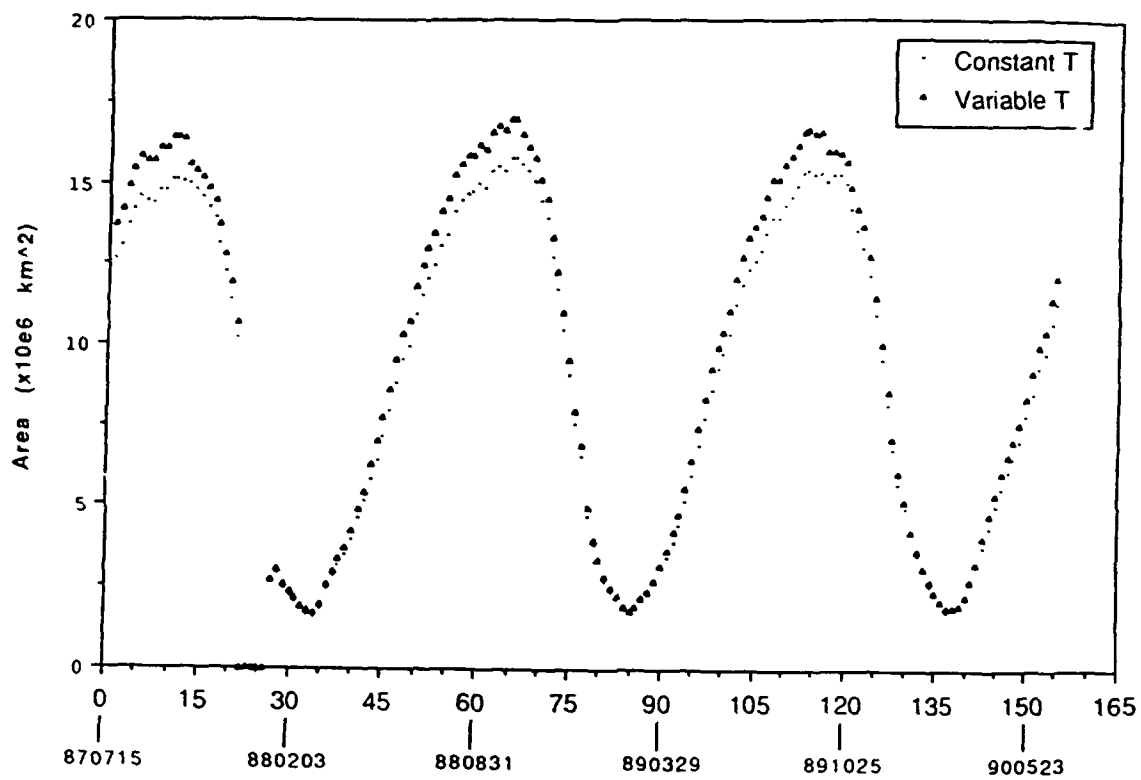
Figure 12. Comparison of the sea ice area predicted by the variable- and constant-temperature NORSEX algorithms.

was essentially identical because the temperature gradients across the ice were almost the same. However, during the winter, the algorithm employing the seasonally-dependent atmospheric temperature produced much higher ice area values. Again, this is because the higher temperature gradient yields higher ice production. The variable-temperature NORSEX algorithm produces results closest to the four-algorithm average. The NASA algorithm generates area values less than the average but still higher than the constant-temperature NORSEX algorithm. The sea-ice area cycle does not show any decreasing trends over the three year period.

Regional Distribution Analysis

Looking at the regional distribution of ice predicted by the algorithms is another method of comparison. For the purpose of these comparisons, the ice pack will be divided into three categories: the marginal ice zone, the coastal zone, and the interior pack. The marginal ice zone refers to the area of low concentrations around the periphery of the ice pack. The coastal zone obviously corresponds to the area immediately adjacent to the continent. Everything between the two other zones is the interior pack and is normally the region of highest ice concentration.

The regional distribution comparisons are based on the images in Figures 13-15. These images show the differences between two algorithms on the same day. They are derived by

(a)

(b)
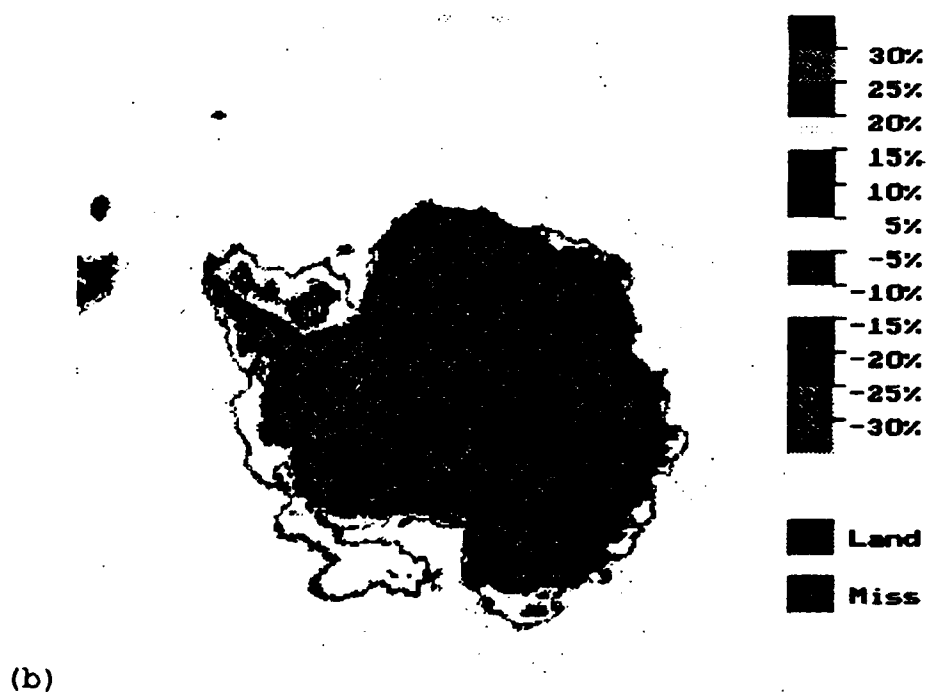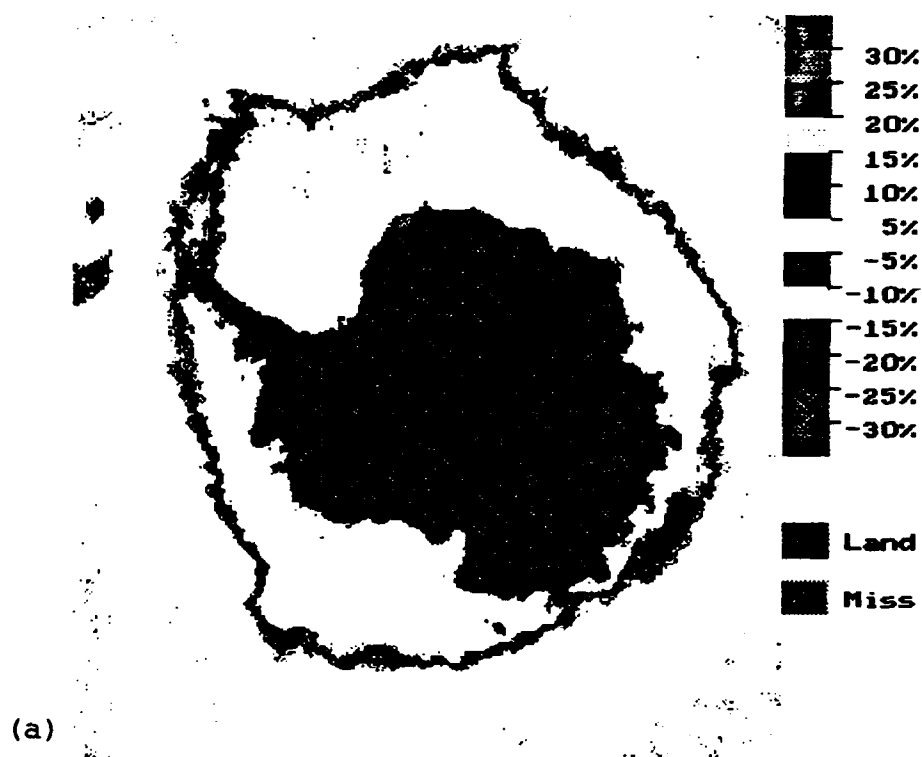
Figure 13. Regional comparison of the variable-temperature
NORSEX and the Comiso algorithms: (a) dated 16 September
1987 and (b) dated 21 February 1988.
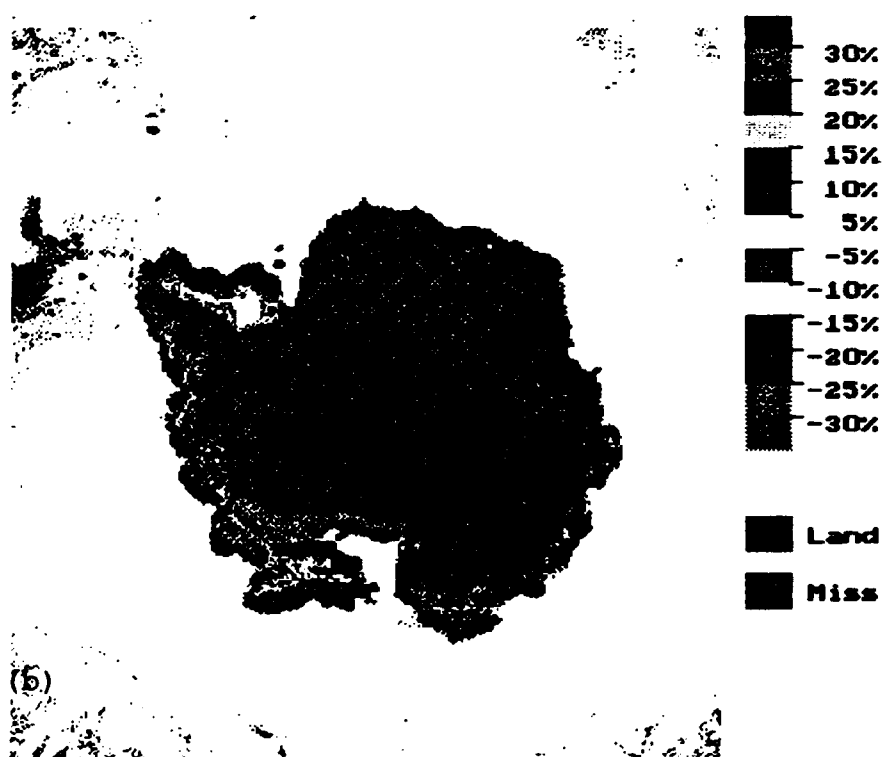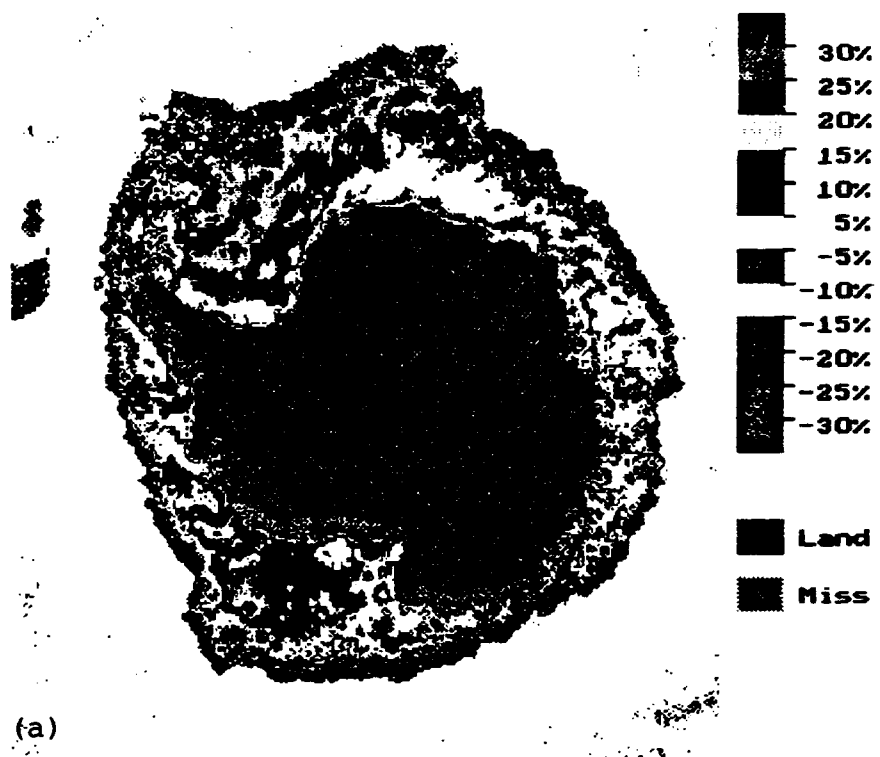
Figure 14. Regional comparison of the variable-temperature NORSEX and the NASA algorithms: (a) dated 16 September 1987 and (b) dated 21 February 1988.

Figure 15. Regional comparison of the Comiso and the NASA algorithms: (a) dated 16 September 1987 and (b) dated 21 February 1988.

taking the ice concentration values from the first algorithm and subtracting the values from the second algorithm. Figures 13-15 show the differences between algorithms on two particular days: 16 September 1987 and 21 February 1988. These days were chosen for comparison because they are representative of the conditions in the winter and summer near the maxima and minima of the sea-ice coverage.

Figure 13 shows the difference between the variable-temperature NORSEX and the Comiso algorithms with the Comiso values subtracted from the NORSEX values. The interior pack has differences less than 5% between the two algorithms. The NORSEX algorithm produces higher concentrations of ice in the marginal ice zone and in coastal zones where the presence of latent heat polynyas are likely. In the summer, however, the Comiso algorithm generates higher concentrations within the remnants of the interior pack. Most of the differences in the winter and the summer are less than 10% concentration with occasional cases as high as 20% and show that the two algorithms are reasonably similar.

The comparisons of the variable-temperature NORSEX and NASA algorithms and the Comiso and NASA algorithms show very large differences in the regional distribution. Figure 14 shows the results from subtracting the NASA from the NORSEX values and Figure 15 the NASA from the Comiso values. The NASA algorithm predicts much smaller concentrations during the winter than the Comiso and NORSEX algorithms in the interior pack - particularly in the Weddell and Ross

Seas. These differences are as high as 30%. Even larger differences occur in the marginal ice zone and the coastal zone throughout the entire year. The NASA algorithm predicts concentrations in excess of 30% below the other two algorithms in the marginal ice zone stretching from the Antarctic Peninsula eastward to about 90° E. Conversely, it exceeds Comiso and NORSEX by more than 30% in the marginal ice zone from the Antarctic Peninsula westward to 90° E. The NASA algorithm predicts higher concentrations than the other two algorithms in the coastal zone around the entire continent. From the Antarctic Peninsula westward to 90° E, this difference is greater than 25%. On the other side of the continent, the differences are not as large, ranging from 5 to 25%. While the NASA algorithm predictions appear similar to the other algorithms when comparing the seasonal sea-ice cycle, the regional distribution comparison indicates that there are significant differences between the algorithms.

Heat Flux Calculations Over Recurring Polynyas

Stewart [1989] has identified several recurring polynyas around Antarctica - most occurring along the coast. Many of these same polynyas appeared in the ice concentration images; however, the polynyas off the Shackleton, Filchner, and Ross ice shelves were the largest and most frequent of these

Figure 16. Location of recurring polynyas used to analyze turbulent heat flux calculations in this project.

polynyas. Figure 16 shows the geographic location of these polynyas. Following the advice of Cavalieri (D. Cavalieri, personal communication), the areas of the polynyas were randomly established and the heat fluxes through those areas were compared for each algorithm. The area of the Shackleton and Filchner polynyas is 8125 km^2 and the area of the Ross polynya is 16250 km^2. The dates chosen for observation include: 21 October 1987, 26 October 1988, and 11 October 1989. These particular dates were chosen because they offered the smallest values of ice concentration and also because these dates precede any influence of the rapid melt that begins in November.

Once the arbitrary polynyas were established, the comparative analysis of the heat fluxes began. The first step involved determining the concentrations of the pixels within the polynya. The heat fluxes in Table 9 are then used to determine the heat flux through each pixel. When ice concentrations fell between the tabulated values, F_I and F_L were determined by linear interpolation and added to give the corresponding value for F_T. The heat flux through an area of open water (0% ice concentration) was assumed to be 300 W m^{-2} [Stewart, 1989; Worby and Allison, 1991]. The fluxes (W m^{-2}) through each pixel were summed and then multiplied by the total area of the polynya (km^2) to give the total heat lost through the polynya (W). The heat lost through the polynya is the basis for the comparison among the algorithms.

Table 9. Area-averaged total heat flux (W m^{-2}) over pack ice for air temperature of -15°C and ice thickness of 0.4 m. F_I is the fractional contribution to the turbulent flux from the ice covered region, F_L is the fractional contribution from open water, and F_T is the average turbulent flux over the entire region [after Worby and Allison, 1991].

Ice Concentration (%)	F_I	F_L	F_T
100	-56	0	-56
80	-45	-89	-134
65	-37	-129	-166
50	-28	-159	-187
30	-17	-182	-199

Figure 17 graphically depicts the results of the heat loss calculations. The total turbulent heat loss is displayed for each polynya by year for 1987-1989. The NASA algorithm yielded the lowest heat loss of the three algorithms in 6 of the 9 observations. While this is not a conclusive pattern, it does indicate that the NASA algorithm has higher ice concentrations most of the time. There is also a pattern of decreasing heat flux over the three-year period in the Filchner Ice Shelf polynya. This corresponds to an increasing trend in the ice coverage in this region, yet the time period is too short to make conclusions regarding any potential effects on the climate. The largest percent difference between the calculations from the Comiso and NORSEX algorithm is 7.5% - indicating the two algorithms

Shackleton Ice Shelf Polynya

Filchner Ice Shelf Polynya

Ross Ice Shelf Polynya
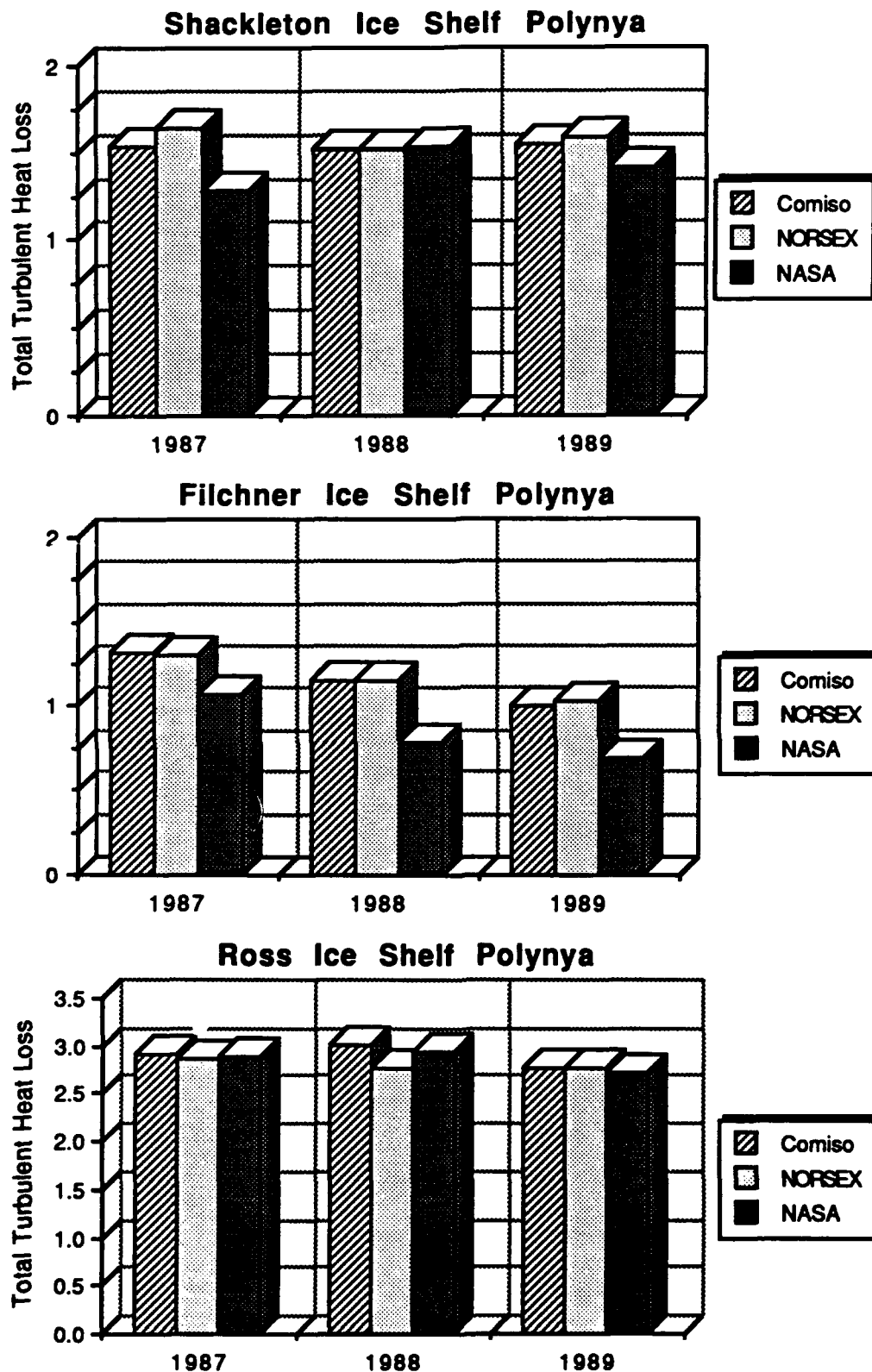
Figure 17. Turbulent heat losses through recurring polynyas. Losses are in units of 1×10^{12} W.

produce very similar results. On the other hand, the percent difference between the NASA algorithm and either the Comiso or NORSEX algorithm is as great as 33%. This further supports the similarity between the Comiso and NORSEX results and questions the accuracy of the NASA results.

FRAM Model

Numerical models currently used in climate prediction have resolutions on the order of hundreds of kilometers. These resolutions are much too coarse to represent major ocean currents and oceanic eddy fields - important mechanisms in the transport of heat in the oceans [*Webb et al.*, 1990]. Coarse models are not capable of properly representing sea-ice concentration and features such as polynyas and leads. *Zwally et al.* [1983] suggest that climatic changes in global average temperature will be evident in the variation of the areal coverage of Antarctic sea ice. In order to improve predictions of climatic change and enhance the understanding of the physics controlling oceanic processes, models must be able to resolve phenomena on the order of tens of kilometers.

A group of scientists in the United Kingdom have developed an eddy-resolving model of the Southern Ocean called the Fine Resolution Antarctic Model (FRAM). The FRAM Group chose to model the Southern Ocean because of the region's influence on the world-wide climate. It is the only

connection between the main ocean basins [*FRAM Group*, 1991].
The model produces data sets for such parameters as stream
function, ocean temperature, current velocity fields, sea-ice
concentration, and ice thickness in grid sizes of 1/2°
longitude by 1/4° latitude. The eddy-resolving portion of
the model is based on *Semtner* [1974] and *Cox* [1984] and was
initialized as a cold (-2°C), saline (36.69 ppt), motionless
fluid and then dynamically relaxed to temperature and
salinity fields based on field measurements by *Levitus* [1982]
[*FRAM Group*, 1991]. The model is forced by annual mean winds
from *Hellerman and Rosenstein* [1983] [*FRAM Group*, 1991].

The sea-ice portion of the model is a modification of
the dynamic-thermodynamic model by *van Ypersele* [1986] (R.
Williams, personal communication). The thermodynamic aspect
of the model is based on *Semtner* [1986] and incorporates a
simple mixed layer, ice growth and melt at the top and bottom
of the ice, latent heat storage in brine pockets, and lateral
melting in leads [*van Ypersele*, 1986]. A simple model of
sea-ice dynamics by *Thorndike and Colony* [1982] is employed
to account for the transport and convergence-divergence of
the ice [*van Ypersele*, 1986]. Integrated over a span of five
model years and forced by a constant oceanic heat flux of 2 W
m^{-2}, the thermodynamic-dynamic model accurately simulated the
seasonal cycle of ice extent as compared to satellite
observations [*van Ypersele*, 1986].

The FRAM Group was able to amass 21 months of model time
for the sea-ice model before their computer allocation time

expired. During the first year of simulation, very little
ice formed due to the intermediate and deep waters being too
warm and fresh [*Stevens*, 1991]. The second year of
simulation proved much better; however, two obvious problems
still exist: the warming of the surface waters of the
Weddell Sea and the advection of ice along the Antarctic
Peninsula [*Stevens*, 1991]. It is believed that these
problems arose due to the type of forcing used for the model.

One objective of this project was to compare the output
of the FRAM sea-ice model with data available from satellite
observations. Several aspects of the model data that were
provided left this objective unattainable. First of all,
nearly the entire ice pack consisted of 98-99% ice with no
polynyas present. The one exception was a large area of open
water occupying most of the Ross Sea. The model did not
produce a continuous marginal ice zone around the pack. Many
portions of the horizontal ice-ocean interface changed from
99% ice to open water across the span of one pixel. The
homogeneity of the ice pack and the lack of a continuous
marginal ice zone reduce the credibility of the model
results. Another problem is the deficiency of the extent of
the ice pack - particularly in the Weddell Sea and Ross Sea
regions. The inaccuracies of the model output have rendered
a quantitative comparison to satellite observations
unnecessary as the differences are obviously apparent. The
inaccuracies of the FRAM sea-ice model will probably be
reduced with increased model integration time just as the

model results of *van Ypersele* [1986] improved with time.
Future comparisons should be pursued upon the availability of
model results that have been integrated over a longer period
of time.

Conclusions

Because no large-scale *in situ* measurements exist, it is
not possible to determine which of the three algorithms is
correct. It is possible, but not very likely, that all three
could be wrong. It is possible, however, to compare the
algorithm results in order to determine where discrepancies
lie. This was the approach of this project. The following
list summarizes the observations and conclusions regarding
the algorithm comparison and heat flux determinations:

1. The Comiso algorithm consistently produces the
highest values of sea-ice extent and area.

2. The variable-temperature NORSEX algorithm produces
more believable results than the constant-temperature version
of the algorithm. This demonstrates the heavy dependence of
ice formation upon the temperature gradient across the ice.

3. The Comiso and variable-temperature NORSEX
algorithms predict very similar ice concentrations (< 5%
difference). Differences as great as 15% do exist, though,
in the marginal ice zone and in regions of coastal polynyas
with the NORSEX algorithm giving higher values.

4. Large disparities are apparent when comparing the NASA algorithm with the Comiso and NORSEX algorithms. Very large differences, some higher then 30%, exist in the marginal ice zones, along the coast, and in the Weddell and Ross Seas.

5. The variable-temperature NORSEX algorithm produces the ice area values most like the average prediction from all of the algorithms.

6. Turbulent heat flux calculations do not reveal a conclusive pattern. The NASA algorithm did produce the lowest heat flux in the majority of the cases.

Several areas of further research have evolved from this project. A long-term analysis of sea-ice coverage should be conducted upon the availability of data. Observations from a 3-year term are not sufficient to determine potential climatic trends. Each of the algorithms use different methods to represent the same phenomenon. Attempts should be made to incorporate the different methods into one algorithm. Employing several calculation mechanisms into one algorithm would hopefully reduce errors and increase the validity of the predictions. The large disparities in predictions in the marginal ice zones and along the coast should be examined to determine the cause of these disparities and to correct them. Finally, algorithm results should be compared to model predictions upon the availability of better model data. Noting the discrepancies between the model and algorithm

results would increase our overall knowledge of the ocean-ice-atmosphere system.

References

Andreas, E.L., Estimation of heat and mass fluxes over arctic leads, *Monthly Weather Review*, 108, 2057-2063, 1980.

Andreas E.L. and B. Murphy, Bulk transfer coefficients for heat and momentum over leads and polynyas, *Journal of Physical Oceanography*, 16, 1875-1883, 1986.

Brown, R.A., Meteorology, in *Polar Oceanography, Part A: Physical Science*, p. 19, Academic Press, Inc., San Diego, CA, 1990.

Carsey, F.D. and H.J. Zwally, Remote sensing as a research tool, in *The Geophysics of Sea Ice*, edited by N. Untersteiner, pp. 1031-1034, Plenum Press, New York, 1986.

Comiso, J.C., Satellite remote sensing of the polar oceans, *Journal of Marine Systems*, 2, 395-434, 1991.

Comiso, J.C. and A.L. Gordon, Recurring polynyas over the Cosmonaut Sea and the Maud Rise, *Journal of Geophysical Research*, 92(C3), 2819-2833, 1987.

Comiso, J.C. and C.W. Sullivan, Satellite microwave and in situ observations of the Weddell Sea-ice cover and its marginal ice zone, *Journal of Geophysical Research*, 91(C8), 9663-9681, 1986.

Cox, M.D., A primitive equation, three-dimensional model of the ocean, *GFDL Ocean Group Technical Report, 1*, Geophysical Fluid Dynamics Laboratory, Princeton University, Princeton, NJ, 1984.

FRAM Group, An eddy-resolving model of the Southern Ocean, *Eos Transactions AGU*, 72(15), 169, 174-175, 1991.

Gordon, A.L. and J.C. Comiso, Polynyas in the southern ocean, *Scientific American*, 258(5), 90-97, 1986.

Gow, A.J. and W.B. Tucker III, Sea ice in the polar regions, *Polar Oceanography, Part A: Physical Science*, pp. 88-90, Academic Press, Inc., San Diego, CA, 1990.

Gow, A.J., D.A. Meese, D.K. Perovich, and W.B. Tucker III, The anatomy of a freezing lead, *Journal of Geophysical Research*, 95(C10), 18229, 1990.

Guth, P.L., *Manipulating large gridded data sets on a personal computer*, FDC [Federal Digital Cartography] Newsletter, 12, 12-14, 1990.

Hall, D.K. and J. Martinec, *Remote Sensing of Ice and Snow*, pp. 14-15 and 159-160, Chapman and Hall, 1985.

Hellerman, S. and M. Rosenstein, Normal monthly wind stress over the world ocean with error estimates, *Journal of Physical Oceanography*, 13, 1093, 1983.

Levitus, S., Climatological atlas of the world ocean, *NOAA Prof. Paper. 13*, Geophysical Fluid Dynamics Laboratory, Princeton University, Princeton, NJ, 1982.

Massom, R.A., The study of Weddell Sea ice using passive microwave and buoy data, pp. 36-52, Ph.D. Thesis, Cambridge University, 1989.

Maykut, G.A., Energy exchange over young ice in the central arctic, *Journal of Geophysical Research*, 83(C7), 3646-3648, 1978.

Muench, R.D., Mesoscale phenomena in the polar oceans, *Polar Oceanography, Part A: Physical Science*, pp. 273-278, Academic Press, Inc., San Diego, CA, 1990.

NASA, Air-sea interaction with SSM/I and altimeter, *Report of the NASA Ocean Energy Fluxes Science Working Group*, pp. 17-18, Jet Propulsion Laboratory, Pasadena, CA, 1985.

National Climatic Data Center, *Joint U.S. Navy/U.S. Air Force climatic study of the upper atmosphere, vol. 1-12*, p. 131, Naval Oceanographic Command Detachment, Asheville, NC, 1989.

National Snow and Ice Data Center, *DMSP SSM/I brightness temperature grids for the polar regions on CD-ROM*, pp. D-1 - D-2, National Snow and Ice Data Center, Boulder, CO, 1990.

Parkinson, C.L., J.C. Comiso, H.J. Zwally, D.J. Cavalieri, P. Gloersen, and W.J. Campbell, *Arctic sea ice, 1973-1976: satellite passive-microwave observations*, pp. 41-45, NASA, Washington, D.C., 1987.

Robinson, I.S., *Satellite oceanography: an introduction for oceanographers and remote-sensing scientists*, p. 263, Ellis Horwood Ltd., 1985.

Semtner, A.J., An oceanic general circulation model with bottom topography, *UCLA Dept. of Meteorology Technical Report, 9*, 99 pp., 1974.

Semtner, A.J., A model for the thermodynamic growth of sea ice in numerical investigations of climate, *Journal of Physical Oceanography*, 6, 379-389, 1976.

Stevens, D., Sea ice, *FRAM News*, 1, 2, 1991.

Stewart, F.H., The distribution and ecological significance of major recurring polynyas, pp. 22-34 and 68-76, M.S. Thesis, 1989.

Stringer, W.J., D.G. Barnett and R.H. Godin, *Handbook for sea ice analysis and forecasting*, p. V-22, Geophysical Institute, University of Alaska, Juneau, AK, 1984.

Svendsen, E., K. Kloster, B. Farrelly, O.M. Johannessen, J.A. Johannessen, W.J. Campbell, P. Gloersen, D. Cavalieri, and C. Matzler, Norwegian remote sensing experiment: evaluation of the Nimbus 7 scanning multichannel microwave radiometer for sea-ice research, *Journal of Geophysical Research*, 88(C5), 2781-2784, 1983.

Thorndike, A.S. and R. Colony, Sea-ice motion in response to geostrophic winds, *Journal of Geophysical Research*, 87, 5845-5852, 1982.

Thorpe, M.R., E.G. Banke, and S.D. Smith, Eddy correlation measurements of evaporation and sensible heat flux over arctic sea ice, *Journal of Geophysical Research*, 78, 3573-3584, 1973.

van Ypersele, Jean-Pascal, A numerical study of the response of the Southern Ocean and its sea ice to a CO_2-induced atmospheric warming, pp. 60-80, Cooperative Thesis 99, Universite Catholique de Louvain-la-Neuve, Belgium and National Center for Atmospheric Research, Boulder, CO, 1986.

Weaver, R., C. Morris, R.G. Barry, and V.J. Troisi, Passive microwave data for snow and ice research: planned products from the DMSP SSM/I system, pp. 134-138, status report from the NOAA conference, Williamsburg, VA., 1-4 June 1987.

Webb, D.J., B.A. de Cuevas, P.D. Killworth, and M. Rowe, Initial results from a fine resolution model of the Southern Ocean, *Internal Document No. 293,* p. 5, Institute of Oceanographic Sciences Deacon Laboratory, Wormley, England, 1990.

Weeks, W.F. and S.F. Ackley, The growth, structure, and properties of sea ice, *The Geophysics of Sea Ice,* edited by N. Untersteiner, pp. 22-51, Plenum Press, New York, 1986.

Worby, A.P. and I. Allison, Ocean-atmosphere energy exchange over thin, variable concentration Antarctic pack ice, *Annals of Glaciology,* 15, 184-190. ·ı.

World Meteorological Organization, *Sea-ice Nomenclature,* World Meteorological Organization, Geneva, 1970.

Zwally, H.J., C.L. Parkinson, J.C. Comiso, Variability of Antarctic sea ice and changes in carbon dioxide, *Science,* 220(4601), 1005-1006, 1983.

Zwally, H.J., J.C. Comiso, and A.L. Gordon, Antarctic offshore leads and polynyas and oceanographic effects, in *Oceanology of the Antarctic Continental Shelf, Antarctic Research Series 43,* pp. 203-226, American Geophysical Union, Washington, D.C., 1985.

Appendix A. Computer Program

```
(*
   ($Define ImageOptions)
   ($Define GraphOptions)
   ($Define ExcludeLandMask)
*)
   ($Define IncludeComisoAlgorithm)

uses
   PETDef,PETMARS,
($IfDef GraphOptions)
   PETGraph,
($EndIf)
($IfDef ImageOptions)
   DrawMain,
($EndIf)
   Graph,
   DOS,CRT;

type
   RowBytes = array[1..316] of byte;
   float = extended;
var
($IfDef ExcludeLandMask)
($Else)
   AntyMask : array[1..332] of ^RowBytes;
($EndIf)
   AlgExt   : string[4];
   AlgCh    : char;
   ShowMap  : boolean;
   IceColorChoices : array[0..255] of byte;
($IfDef GraphOptions)
   TempRec1,
   TempRec2 : array[150..300] of LongInt;
($EndIf)


procedure IceColorCuts;
var
   i,j : integer;
begin
   SetVGAColor(14,63,63,0);
   SetVGAColor(15,63,63,63);
   for i := 0 to 5 do IceColorChoices[i] := 0;
   for j := 0 to 8 do
      for i := 6+ j*10 to 15+j*10 do IceColorChoices[i] := succ(j);
   for i := 95 to 255 do IceColorChoices[i] := 10;
   IceColorChoices[157] := 14;
   IceColorChoices[168] := 15;
end;
```

```
procedure ProcessFile(FName,OutName : PathStr);
var
    Infile : file;
    Outfile : file;
    NumRecords,i,j        : integer;
    InputArray : array[1..316*5] of integer;
    OutputArray1,
    OutputArray2  : array[1..5,1..316] of integer;
    CalcValues    : array[1..316] of byte;
    MonthStr      : string[2];
    Month,Error   : integer;


    Dir : DirStr;
    Name : NameStr;
    Ext  : ExtStr;



procedure NASAalgorithm;
label
      WATER,
      BadData;
var

  (Tie Point Brightness Temperatures)

    TB19VW,
    TB19VF,
    TB19VM,
    TB19HW,
    TB19HF,
    TB19HM,
    TB37VW,
    TB37VF,
    TB37VM,

  (Sums and Differences of Tie Points)

    DWA,
    DFA,
    DMA,
    SWA,
    SFA,
    SMA,
    DWB,
    DFB,
    DMB,
    SWB,
    SFB,
    SMB,
    TB19V,          (19V GHz Brightness Temperature)
    TB19H,          (19H GHz Brightness Temperature)
    TB37V,          (37V GHz Brightness Temperature)
    FYICE,          (First-year Ice Fraction)
```

```
    MYICE,              (Multiyear Ice Fraction)
    TOTICE,             (Total Ice Concentration)
    GR,                 (Gradient Ratio)
    PR,                 (Polarization Ratio)
    PRGR,               (Product of Polarization and Gradient Ratios)
    ANF,
    ANM,
    DD    :   float;
    C     :   array[1..12] of float;          (Coefficients)

Begin

  (Tie Point Brightness Temperatures)

    TB19VW := 175.3;
    TB19HW := 97.7;
    TB19VF := 251.2;
    TB19HF := 241.7;
    TB19VM := 223.2;
    TB19HM := 203.9;
    TB37VW := 199.6;
    TB37VF := 248.3;
    TB37VM := 186.3;


  (Calculation of Sums and Differences of Tie Points)

    DWA := TB19VW - TB19HW;
    DFA := TB19VF - TB19HF;
    DMA := TB19VM - TB19HM;
    SWA := TB19VW + TB19HW;
    SFA := TB19VF + TB19HF;
    SMA := TB19VM + TB19HM;
    DWB := TB37VW - TB19VW;
    DFB := TB37VF - TB19VF;
    DMB := TB37VM - TB19VM;
    SWB := TB37VW + TB19VW;
    SFB := TB37VF + TB19VF;
    SMB := TB37VM + TB19VM;


  (Calculation of Coefficients)

    C[1]  := DMA*DWB - DMB*DWA;
    C[2]  := DMB*SWA - DWB*SMA;
    C[3]  := DWA*SMB - DMA*SWB;
    C[4]  := SMA*SWB - SMB*SWA;
    C[5]  := DFA*(DMB-DWB) + DWA*(DFB-DMB) + DMA*(DWB-DFB);
    C[6]  := DFB*(SMA-SWA) + DWB*(SFA-SMA) + DMB*(SWA-SFA);
    C[7]  := DFA*(SWB-SMB) + DWA*(SMB-SFB) + DMA*(SFB-SWB);
    C[8]  := SFB*(SWA-SMA) + SWB*(SMA-SFA) + SMB*(SFA-SWA);
    C[9]  := DFB*DWA - DFA*DWB;
    C[10] := DWB*SFA - DFB*SWA;
    C[11] := SWB*DFA - DWA*SFB;
    C[12] := SFB*SWA - SFA-SWB;
```

```
(Read Data)

   TB19V := 0.1 * OutPutArray1[1,i];
   TB19H := 0.1 * OutPutArray1[2,i];
   TB37V := 0.1 * OutPutArray1[4,i];

(Check for Missing Data)

   If (TB19V < 0.0001) or (TB19H < 0.0001) or (TB37V < 0.0001) then
     Begin
          CalcValues[i] := 157;
        Goto BadData;
        End
     Else Begin

(Open Water Weather Filter)

          GR := (TB37V - TB19V)/(TB37V + TB19V);
          If GR > 0.05 then
             Begin
                  FYICE := 0.0;
                  MYICE := 0.0;
                  TOTICE := 0.0;
                GOTO WATER;
                End
             Else Begin

(Noniterative Ice Algorithm)

                  PR := (TB19V - TB19H)/(TB19V + TB19H);
                  PRGR := PR * GR;
                  ANF := C[1] + C[2]*PR + C[3]*GR + C[4]*PRGR;
                  ANM := C[9] + C[10]*PR + C[11]*GR + C[12]*PRGR;
                  DD := C[5] + C[6]*PR + C[7]*GR + C[8]*PRGR;

                  FYICE := 100 * (ANF/DD);
                  MYICE := 100 * (ANM/DD);
                  TOTICE := FYICE + MYICE;
             End;

(Set Concentrations >100% to 100% and <0% to 0%)

          If TOTICE <= 0.0001 then
            begin
                 TOTICE := 0.00;
            end;
          If TOTICE >= 100.0 then
            begin
                 TOTICE := 100.0;
            end;

   WATER:;
   CalcValues[i] := round(TOTICE);
   BadData:;
```

```pascal
        End;
End;




procedure NORSEXalgorithm(Col : integer);
label
        WATER;

const
        Taus19    = 0.04;    {Atmospheric Opacity for 19 GHz in the subarctic}
        Taus37    = 0.10;    {Atmospheric Opacity for 37 GHz in the subarctic}
        Taua19    = 0.03;    {Atmospheric Opacity for 19 GHz in the arctic}
        Taua37    = 0.07;    {Atmospheric Opacity for 37 GHz in the arctic}
        Tune19    = 2.0;     {"Tune" Factor for Brightness Temp at 19 GHz}
        Tune37    = 8.0;     {"Tune" Factor for Brightness Temp at 37 GHz}
        p1        = 250.0;
        p2        = 20.0;
        p3        = 2.0;
        p4        = 1.0;
        p5        = 2.0;
        ew19      = 0.621;   {Water Emissivity at 19 GHz}
        ew37      = 0.712;   {Water Emissivity at 37 GHz}
        ef19      = 0.95;    {First-year Ice Emissivity at 19 GHz}
        ef37      = 0.95;    {First-year Ice Emissivity at 37 GHz}
        em19      = 0.80;    {Multiyear Ice Emissivity at 19 GHz}
        em37      = 0.65;    {Multiyear Ice Emissivity at 37 GHz}
        tapi      = 260.0;   {Atmospheric Surface Temp Over 100% Ice}
var
    Ta:  array[0..2] of float;   {Atmospheric surface temp over open water}
    tau19,                       {Interpolated Atmospheric Opacity for 19 GHz}
    tau37,                       {Interpolated Atmospheric Opacity for 37 GHz}
    tba19,
    tba37,

    ()

    a11,
    a12,
    a21,
    a22,
    c1,
    c2,
    d,
    cm,                     {MY ice concentration}
    cf,                     {FY ice concentration}
    ct:  array[1..2] of float;   {Total ice concentration}

    tice,                   {Physical Temprature of Ice}
    tw19,                   {Brightness Temp of Water at 19 GHz}
    tw37,                   {Brightness Temp of Water at 37 GHz}
    tf19,                   {Brightness Temp of FY Ice at 19 GHz}
    tf37,                   {Brightness Temp of FY Ice at 37 GHz}
    tm19,                   {Brightness Temp of MY Ice at 19 GHz}
```

```
    tm37,                    (Brightness Temp of MY Ice at 37 GHz)
    tb19,                    (Raw Data Brightness Temp for 19 GHz)
    tb37,                    (Raw Data Brightness Temp for 37 GHz)
    tbh19,                   (Calibrated Brightness Temp for 19 GHz)
    tbh37,                   (Calibrated Brightness Temp for 37 GHz)
    GR        : float;       (Gradient Ratio)
    i         : integer;
begin

  (Atmospheric Temperature That Varies with Season)

     Ta[0]       := 263.0;

  (Read Data)

     Tb19 := 0.1 * OutPutArray1[1,Col];
     Tb37 := 0.1 * OutPutArray1[4,Col];

  (Check for Missing Data)

     If (tb19 <= 0.0001) or (tb37 <= 0.0001) then
       begin
         CalcValues[col] := 157;
         goto WATER;
       end

     else

  (Calibration of Raw Data)

         Tbh19 := Tb19 + Tune19;
         Tbh37 := Tb37 + Tune37;

  (Calculation of Brightness Temperatures)

         Tice := 0.4*Ta[0] + 0.6*272;
         Tw19 := ew19*Ta[0];
         Tw37 := ew37*Ta[0];
         Tf19 := ef19*Tice;
         Tf37 := ef37*Tice;
         Tm19 := em19*Tice;
         Tm37 := em37*Tice;

  (Open Water Weather Filter)

     GR := (Tbh37 - Tbh19)/(Tbh37 + Tbh19);
     If GR > 0.05 then
        begin
        CalcValues[col] := 0;
        goto WATER;
        end
     else

  (Ice Concentration Algorithm)
```

```
            for i := 1 to 2 do
              begin
                Tau19[i] := (Taua19 + (Ta[i-1] - p1)*(Taus19 - Taua19))/p2;
                Tba19[i] := (Tbh19 - Ta[i-1]*(p3*Tau19[i] - p4*sqr(Tau19[i]) +
                    0.01))/(1 - p5*Tau19[i] + (p5-1)*sqr(Tau19[i]) - 0.01);
                Tau37[i] := (Taua37 + (Ta[i-1] - p1)*(Taus37 - Taua37))/p2;
                Tba37[i] := (Tbh37 - Ta[i-1]*(p3*Tau37[i] - p4*sqr(Tau37[i]) +
                    0.01))/(1 - p5*Tau37[i] + (p5-1)*sqr(Tau37[i]) - 0.01);

                a11[i]  := Tf19 - Tw19;
                a12[i]  := Tf37 - Tw37;
                a21[i]  := Tm19 - Tw19;
                a22[i]  := Tm37 - Tw37;
                c1[i]   := Tba19[i] - Tw19;
                c2[i]   := Tba37[i] - Tw37;
                d[i]    := a11[i]*a22[i] - a12[i]*a21[i];
                cm[i]   := (a11[i]*c2[i] - a21[i]*c1[i])/d[i];
                cf[i]   := (a22[i]*c1[i] - a12[i]*c2[i])/d[i];
                ct[i]   := cf[i] + cm[i];
                Ta[i]   := Ta[i-1] + (Tapi - Ta[i-1])*ct[i];
              end;

      (Set Concentrations >100% to 100% and <0% to 0%)

          If ct[2] <= 0.00001 then
            begin
            ct[2] := 0.0;
          - end
          else
          If ct[2] >= 1.0 then
            begin
            ct[2] := 1.0;
            end
          else

            CalcValues[Col] := round(100 * ct[2]);
            WATER:;
end;




($IfDef IncludeComisoAlgorithm)

procedure ComisoAlgorithm;
  label
    WaterPixel,
    BadData;
  var
    GR,              (Gradient Ratio)
    A1,              (Intercept for Consolidated Ice Line)
    A2,              (Slope for Consolidated Ice Line)
    WTP1,            (37V GHz Water Tie Point)
    WTP2,            (19V GHz Water Tie Point)
```

```
        TTP1,               (37V GHz Consolidated Ice Tie Point)
        TTP2,               (19V GHz Consolidated Ice Tie Point)
        WINTRC,             (Intercept of 100% Water Line)
        WSLOPE,             (Slope of 100% Water Line)
        ICEC,               (Ice Concentration)
        RADT2,              (Radius of Circle of 100% Ice)
        TTPS,               (Slope of Line Between Water and Ice Tie Points)
        TTPI,               (Intercept of Line Between Water and Ice Tie Points)
        TTPR,               (Arctangent of TTPS)
        ET1,                (Y-Coordinate of Solution to Water Line)
        ET2,                (Y-Coordinate of Solution to Water-Ice Line)
        ED,                 (Difference Between TB1 and WTP1)
        EINT1,              (Y-Coordinate of Point of Intersection)
        EINT2,              (Y-Coordinate of Point of Intersection)
        BET,                ()
        ALP,                ()
        SLDVH,              ()
        CTHTA,              ()
        TB1,                (37V GHz Brightness Temperature)
        TB2,                (19V GHz Brightness Temperature)
        RINT,               (Distance from Consolidated Ice Line to Water)
        RI,                 (Distance from Data Point to Water)
        CON   :   FLOAT;
Begin

   (Read Data)

       TB1 := 0.1 * OutPutArray1[4,i];
       TB2 := 0.1 * OutPutArray1[1,i];

   (Check for Missing Data)

       If (TB1 <= 0.0001) or (TB2 <= 0.0001) then
          Begin
               CalcValues[i] := 157;
               Goto BadData;
          End;

($IfDef GraphOptions)
       if not ShowMap then begin
          PutPixel(ScreenX(TB1),ScreenY(TB2),LightGreen);
          if (round(TB1) >= 150) and (round(TB1) <= 300) then inc(TempRec1[round(TB1)]);
          if (round(TB2) >= 150) and (round(TB2) <= 300) then inc(TempRec2[round(TB2)]);
       end (if);
($EndIf)


(Constants for Algorithm)

       case Month of
       3..10       : A1 := 146.75;   (Intercept of Consolidated Ice Line)
       1..2,11..12 : A1 := 145.75;
       end;


       A2    := 0.45;            (Slope of Consolidated Ice Line)
```

```
WTP1    := 205.0;          (37V GHz Water Tie Point)
WTP2    := 182.0;          (19V GHz Water Tie Point)
TTP1    := 262.0;          (37V GHz FY Ice Tie Point)
TTP2    := 256.0;          (19V GHz FY Ice Tie Point)
WINTRC  := 21.0;           (Intercept of 100% Water Line)
WSLOPE  := 0.80;           (Slope of 100% Water Line)
ICEC    := 0;              (Ice Concentration as Fraction)
CON     := 0;              (Ice Concentration as Percentage)

(Ice Concentration Algorithm)

RADT2 := SQRT(sqr(WTP1-TTP1) + sqr(WTP2-TTP2));
TTPS  := (TTP2-WTP2)/(TTP1-WTP1);
TTPI  := TTP2 - TTPS*TTP1;
TTPR  := ARCTAN(TTPS);


ET1   := WSLOPE*TB1 + WINTRC;
IF ET1 > TB2 THEN GOTO WATERPIXEL;
ET2   := TTPS*TB1 + TTPI;
ED    := TB1 - WTP1;


IF abs(ED) <= 0.00001  THEN
   BEGIN
      EINT1 := WTP1;
    · EINT2 := A1 + A2*EINT1;
   END
   ELSE
   Begin
      IF (ET2 <= TB2) OR (abs(A1) < 0.0001) OR (RADT2 <= 0)  THEN
         BEGIN
            BET   := (TB2 - WTP2)/ED;
            ALP   := TB2 - BET*TB1;
            SLDVH := A2 - BET;
            IF abs(SLDVH) < 0.0001 THEN GOTO WATERPIXEL;
            EINT1 := (ALP - A1)/SLDVH;
            EINT2 := A1 + A2*EINT1;
         END
         ELSE
            Begin
               CTHTA := COS(TTPR);
               EINT1 := CTHTA*RADT2 + WTP1;
               EINT2 := TTPI + EINT1*TTPS;
            END;
      END;

RINT := SQRT(sqr(EINT1 - WTP1) + sqr(EINT2 - WTP2));
IF abs(RINT) < 0.00001 THEN GOTO WATERPIXEL;
RI   := SQRT(sqr(TB1 - WTP1) + sqr(TB2 - WTP2));
ICEC := RI/RINT;
CON  := ICEC *100;

(Set Concentrations >100% to 100% and <0% to 0%)

If CON <= 0.0001 then
```

```
            Begin
                CON := 0.0;
            end;


        If CON >= 100.0 then
            Begin
                CON := 100.0;
            end;


    WaterPixel:;
    CalcValues[i] := round(CON);
    BadData:;
end;
($EndIf)


var
($IfDef GraphOptions)
    MaxHorizAxis,MinHorizAxis,
    MaxVertAxis,MinVertAxis        : float;
    HorizCycleCuts,VertCycleCuts  : CycleCutType;
    NumHorizCycles,NumVertCycles  : integer;
($EndIf)
    Screen2Preserved : boolean;
    MaxCount         : LongInt;
begin
    SelectGraphicsMode;
    Screen(500,50,Yellow,AlgExt);
    FSplit(FName,Dir,Name,Ext);
    MonthStr .= Copy(Name,3,2);
    Val(MonthStr,Month,Error);
    Screen(100,ScreenYMax -10,LightGreen,FName);
($IfDef GraphOptions)
    if not ShowMap then begin
        MinHorizAxis := 150;
        MaxHorizAxis := 300;
        MinVertAxis := 150;
        MaxVertAxis := 300;
        FillChar(TempRec1,SizeOf(TempRec1),0);
        FillChar(TempRec2,SizeOf(TempRec2),0);
        ForceLinearAxisFit(HorizCycleCuts[1,1],NumHorizCycles,
            MinHorizAxis,MaxHorizAxis);
        ForceLinearAxisFit(VertCycleCuts[1,1],NumVertCycles,
            MinVertAxis,MaxVertAxis);
        CreateGraphAxes(Linear,Linear,MinHorizAxis,MaxHorizAxis,MinVertAxis,
            MaxVertAxis,NumHorizCycles,NumVertCycles,Cyan,HorizCycleCuts[1,1],
            VertCycleCuts[1,1],'','',FullGrid);
    end;
($EndIf)
    assign(Infile,FName);
    reset(Infile,2*5*316);
    assign(OutFile,OutName);
    rewrite(OutFile,316);
    NumRecords := 0;
    delay(100);
```

```
   while not EOF(Infile) do begin
      BlockRead(Infile,InputArray,1);
      inc(NumRecords);
      gotoxy(60,1); writeln('Line:',NumRecords:5);
      for i := 1 to 316 do
         for j := 1 to 5 do
            OutPutArray1[j,i] := InputArray[5*pred(i) + j];


      {calculate a Point}
      for i := 1 to 316 do begin
{$IfDef ExcludeLandMask}
{$Else}
         if AntyMask[NumRecords]^[i] = 255 then begin
            if ShowMap then PutPixel(i,NumRecords,White);
            CalcValues[i] := 168;
         end
         else
{$EndIf}
               begin
               case AlgCh of
{$IfDef IncludeComisoAlgorithm}
                  'C' : ComisoAlgorithm;
{$EndIf}
                  'N' : NORSEXAlgorithm(i);
                  'A' : NasaAlgorithm;
               end;
               if ShowMap then
                  PutPixel(i,NumRecords,IceColorChoices[CalcValues[i]]);
         end;
      end;
      BlockWrite(OutFile,CalcValues,1);
      if KeyPressed then if ReadKey = #27 then halt;
   end;


   if not ShowMap then begin
{$IfDef ImageOptions}
      PETMARImageOption(true,true,PrinterOption,DefaultPrint,'',Screen2Preserved);
{$EndIf}
      SelectGraphicsMode;

{$IfDef GraphOptions}
      MaxCount := 0;
      for i := 150 to 300 do begin
         if TempRec1[i] > MaxCount then MaxCount := TempRec1[i];
         if TempRec2[i] > MaxCount then MaxCount := TempRec2[i];
      end;
      MinHorizAxis := 150;
      MaxHorizAxis := 300;
      MinVertAxis := 0;
      MaxVertAxis := MaxCount;
      ForceLinearAxisFit(HorizCycleCuts[1,1],NumHorizCycles,
         MinHorizAxis,MaxHorizAxis);
      ForceLinearAxisFit(VertCycleCuts[1,1],NumVertCycles,
         MinVertAxis,MaxVertAxis);
```

```
            CreateGraphAxes(Linear,Linear,MinHor.zAxis,MaxHorizAxis,MinVertAxis,
                MaxVertAxis,NumHorizCycles,NumVertCycles,Cyan,HorizCycleCuts[1,1],
                VertCycleCuts[1,1],'','',FullGrid);
            MoveTo(ScreenX(150),ScreenY(0));
            SetColor(LightRed);
            for i := 151 to 300 do LineTo(ScreenX(i),ScreenY(TempRec1[i]));
            MoveTo(ScreenX(150),ScreenY(0));
            SetColor(LightBlue);
            for i := 151 to 300 do LineTo(ScreenX(i),ScreenY(TempRec2[i]));
    {$EndIf}
    {$IfDef ImageOptions}
            PETMARImageOption(true,true,PrinterOption,DefaultPrint,'',Screen2Preserved);
    {$EndIf}
       end;


       close(Infile);
       close(Outfile);
    end;



    var
       OutPutPath,CDROMPath,FName : PathStr;
       FileInfo  : SearchRec;
       Path : DirStr;
       Date : NameStr;
       Ext  : ExtStr;
       MaskFile : file;
       LandMask : array[1..316] of byte;
       YearName : array[1..10] of PathStr;
       MonthName : array[1..12] of PathStr;
       NumYears,NumMonths,i,j,x,y : integer;
    begin
       SelectGraphicsMode;
    {$IfDef ExcludeLandMask}
    {$Else}
       for i := 1 to 332 do begin
          New(AntyMask[i]);
          FillChar(AntyMask[i]^,SizeOf(RowBytes),0);
       end;
    {$EndIf}
       CDROMPath := 'f:\';
       OutPutPath := 'd:\lomax\icefiles\';

       GetDOSPath('CD-ROM data',CDROMPath);
       CursorXY(1,1);
       GetDOSPath('Data file output',OutPutPath);

       ShowMap := AnswerIsYesXY(10,10,'Show map while processing');
    {$IfDef ExcludeLandMask}
    {$Else}
       assign(MaskFile,CDROMPath + 'TOOLS\S3BMASK.DAT');
       reset(MaskFile,316);
       for y := 1 to 332 do begin
          BlockRead(MaskFile,LandMask,1);
```

```
        for x := 1 to 316 do begin
            if LandMask[x] > 0 then begin
                PutPixel(x,y,15);
                AntyMask[y]^[x] := 255;
            end;
        end;
    end;
    close(MaskFile);
(SEndIf)


(*
    assign(MaskFile,CDROMPath + 'TOOLS\S3BCOAST.DAT');
    reset(MaskFile,316);
    for y := 1 to 332 do begin
        BlockRead(MaskFile,LandMask,1);
        for x := 1 to 316 do begin
            if LandMask[x] > 0 then PutPixel(x,y,LightBlue);
        end;
    end;
    close(MaskFile);
*)
(*
    AlgExt := '.COM';
    AlgCh := 'C';
    FName := 'F:\s3b\1989\jan\890119.s3b';
    ProcessFile(FName,'D:\Lomax\Icefiles\890119.COM');
    Halt;
*)


    SelectTextMode;
    i := 3;
    MakeMenu('^Algorithm to use:\^L> All\^Comiso\^NORSEX\^A> NASA',10,10,AlgCh,i);
    case AlgCh of
        'C' : AlgExt := '.COM';
        'N' : AlgExt := '.NOR';
        'A' : AlgExt := '.ASA';
    end;
StartTheTimer;
    IceColorCuts;
repeat
    FindFirst(CDROMPath + 's3b\*.*',Directory,FileInfo);
    NumYears := 0;
    while DOSerror = 0 do begin
        if Length(FileInfo.Name) = 4 then begin
            inc(NumYears);
            YearName[NumYears] := CDROMPath + 's3b\' + FileInfo.Name;
        end;
        FindNext(FileInfo);
    end (while);

    for i := 1 to NumYears do begin
        FindFirst(YearName[i] + '\*.*',Directory,FileInfo);
        NumMonths := 0;
```

```
      while DOSerror = 0 do begin
        if Length(FileInfo.Name) = 3 then begin
          inc(NumMonths);
          MonthName[NumMonths] := YearName[i] + '\' + FileInfo.Name;
        end;
        FindNext(FileInfo);
      end (while);
      for j := 1 to NumMonths do begin
        FindFirst(MonthName[j] + '\*.*',0,FileInfo);
        NumMonths := 0;
        while DOSerror = 0 do begin
          FName := MonthName[j] + '\' + FileInfo.Name;
          FSPlit(FName,Path,Date,Ext);
          if AlgCh = 'L' then begin
            AlgExt := '.ASA';
            AlgCh := 'A';
            ProcessFile(FName,OutPutPath + Date + AlgExt);
            AlgExt := '.COM';
            AlgCh := 'C';
            ProcessFile(FName,OutPutPath + Date + AlgExt);
            AlgExt := '.NOR';
            AlgCh := 'N';
            ProcessFile(FName,OutPutPath + Date + AlgExt);
            AlgCh := 'L';
          end
          else ProcessFile(FName,OutPutPath + Date + AlgExt);
          FindNext(FileInfo);
          if KeyPressed then if ReadKey = #27 then halt;
        end;
      end (while);
    end (for i);
    EndTheTimer(10,10,' process one CD-ROM');
  until Not AnswerIsYesXY(100,ScreenYMax-50,'Process another CD');
  Presskeycontinues;
  {$IfDef ExcludeLandMask}
  {$Else}
    for i := 1 to 332 do Dispose(AntyMask[i]);
  {$EndIf}
end.
```

Appendix B. Sea Ice Extent and Area, July 1987 to June 1990

Week	Comiso (A)	Comiso (Ext)	NASA (A)	NASA (Ext)	NORSEX (A)	NORSEX (Ext)
870715	15.12	17.32	13.16	16.83	13.73	16.38
870722	15.55	18.35	13.47	17.55	14.16	17.08
870729	16.23	18.94	14.31	18.33	14.92	17.89
870805	16.64	19.57	14.67	18.94	15.40	18.42
870812	17.03	20.08	15.25	19.40	15.82	18.84
870819	16.92	20.13	15.20	17.31	15.70	18.85
870826	16.86	19.98	15.15	19.55	15.69	18.98
870902	17.22	20.22	15.40	19.90	16.08	19.25
870909	17.23	20.46	15.38	19.98	16.07	19.29
870916	17.58	21.11	15.51	20.58	16.43	19.91
870923	17.56	20.92	15.65	20.49	16.40	19.78
870930	17.45	20.81	15.51	20.38	16.33	19.73
871007	17.41	20.91	15.29	20.22	15.58	19.52
871014	17.25	20.10	15.16	19.71	15.38	18.98
871021	17.02	20 19	14.92	19.59	15.14	18.77
871028	16.73	19.60	14.59	19.03	14.86	18.27
871104	16.31	19.62	14.10	18.61	14.46	17.87
871111	15.56	18.71	13.29	18.07	13.70	17.24
871118	11.69	17.93	12.42	17.31	12.78	16.43
871125	13.81	17.42	11.54	16.70	11.92	15.85
871202	12.60	17.10	10.34	15.54	10.68	14.66
871209	0.00	0.00	0.00	0.00	0.00	0.00
871216	0.00	0.00	0.00	0.00	0.00	0.00
871223	0.00	0.00	0.00	0.00	0.00	0.00
871230	0.00	0.00	0.00	0.00	0.00	0.00
880106	0.00	0.00	0.00	0.00	0.00	0.00
880113	4.03	4.40	2.99	4.55	2.72	3.86
880120	5.50	6.45	3.36	5.31	3.04	4.73
880127	5.10	5.82	3.01	4.78	2.60	4.17
880203	4.87	5.41	2.70	4.30	2.37	3.77
880210	4.71	5.88	2.50	4.07	2.17	3.51
880217	4.52	5.28	2.37	3.94	1.95	3.31
880224	4.37	5.54	2.25	3.89	1.78	3.28
880302	4.32	5.79	2.16	3.75	1.72	3.17
880309	4.58	6.04	2.40	4.20	2.00	3.61
880316	5.24	10.52	2.96	5.08	2.57	4.27
880323	5.54	7.76	3.23	5.16	3.01	4.64
880330	5.83	6.10	3.60	5.52	3.39	5.04
880406	6.13	6.55	3.84	5.86	3.73	5.44
880413	6.58	7.28	4.29	6.47	4.21	6.07
880420	7.21	8.27	5.03	7.24	4.90	6.87
880427	7.71	9.18	5.47	8.03	5.42	7.61
880504	8.43	10.30	6.21	8.66	6.29	8.28
880511	9.03	10.44	6.90	9.89	7.02	9.18
880518	9.65	10.92	7.53	10.54	7.76	10.15
880525	10.46	11.96	8.26	11.38	8.64	10.97
880601	11.32	12.86	9.28	12.33	9.53	11.89

880608	12.03	13.67	10.04	13.31	10.32	12.85
880615	12.42	14.51	10.44	13.95	10.75	13.46
880622	13.40	16.03	11.41	15.47	11.80	14.88
880629	13.94	16.28	12.16	15.98	12.45	15.68
880706	14.52	16.43	12.74	16.03	13.00	15.57
880713	14.90	17.26	13.06	16.87	13.42	16.34
880720	15.52	17.93	13.63	17.63	14.11	17.06
880727	15.88	18.48	14.08	18.02	14.48	17.48
880803	16.57	18.86	14.78	18.58	15.20	18.06
880810	16.90	19.72	15.24	19.26	15.58	18.70
880817	17.11	19.96	15.25	19.51	15.82	18.97
880824	17.15	19.97	14.98	19.56	15.85	18.99
880831	17.44	21.76	15.30	20.84	16.16	19.92
880907	15.96	19.97	15.21	19.88	16.03	19.25
880914	16.46	21.00	15.58	21.05	16.55	20.19
880921	16.65	20.91	15.61	20.78	16.73	20.21
880928	16.49	20.51	15.54	20.43	16.60	19.73
881005	16.89	20.80	15.96	20.65	16.98	20.00
881012	16.89	20.74	15.93	20.60	16.97	19.97
881019	16.67	20.44	15.68	20.32	16.47	19.62
881026	16.46	20.12	15.46	19.99	16.08	19.32
991102	16.16	19.68	15.08	19.56	15.74	18.91
881109	15.64	19.07	14.56	18.95	15.08	18.23
881116	15.03	18.49	13.91	18.40	14.50	17.65
881123	13.83	17.55	12.90	17.39	13.30	16.60
881130	12.73	16.51	11.87	16.42	12.26	15.68
881207	11.35	15.38	10.58	15.27	10.98	14.55
881214	9.92	14.21	9.36	14.12	9.55	13.39
881221	8.32	12.69	7.94	12.58	7.98	11.65
881228	7.24	11.39	7.07	11.27	6.88	10.36
890104	5.80	9.86	5.19	8.77	4.94	7.89
890111	6.34	8.06	4.18	6.81	3.96	6.11
890118	5.82	6.76	3.66	5.87	3.38	5.31
890125	5.37	7.27	3.26	5.13	2.84	4.60
890201	5.01	6.06	2.91	4.62	2.49	4.11
890208	4.85	7.01	2.75	4.45	2.26	3.87
890215	4.53	5.70	2.49	4.01	1.93	3.42
890222	4.37	4.86	2.31	3.82	1.78	3.24
890301	4.58	6.68	2.44	4.03	1.93	3.43
890308	4.80	6.21	2.65	4.33	2.19	3.77
890315	4.95	5.89	2.81	4.54	2.39	4.05
890322	5.27	6.06	3.06	4.98	2.73	4.47
890329	5.70	5.97	3.45	5.41	3.21	5.00
890405	6.08	8.56	3.76	5.82	3.67	5.45
890412	6.47	7.07	4.22	6.29	4.21	5.95
890419	6.98	7.28	4.80	7.00	4.79	6.64
890426	7.71	8.75	5.60	7.93	5.55	7.52
890503	8.51	11.17	6.52	9.07	6.40	8.66

890510	9.39	10.91	7.40	10.05	7.39	9.64
890517	10.27	12.24	8.25	11.17	8.34	10.74
890524	11.13	12.68	9.29	12.09	9.26	11.67
890531	11.79	13.90	10.03	13.07	9.96	12.55
890607	12.22	13.89	10.47	13.52	10.43	13.00
890614	12.84	14.89	10.91	14.35	11.08	13.87
890621	13.76	15.81	11.90	15.34	12.05	14.84
890628	14.36	16.76	12.50	15.98	12.69	15.49
890705	14.82	16.90	12.89	16.41	13.34	15.88
890712	15.03	17.09	13.02	16.68	13.65	16.19
890719	15.34	17.41	13.42	17.10	14.00	16.60
890726	15.92	18.52	13.83	17.92	14.58	17.24
890802	16.39	18.71	14.47	18.35	15.11	17.82
890809	16.37	19.05	14.60	18.73	15.13	18.12
890816	16.76	19.61	14.96	19.17	15.53	18.55
890823	17.01	19.96	15.32	19.55	15.82	18.92
890830	17.36	20.28	15.77	19.85	16.18	19.29
890906	17.75	20.38	15.84	19.97	16.57	19.37
890913	17.79	20.51	15.86	19.98	16.61	19.38
890920	17.66	20.34	15.69	19.98	16.52	19.41
890927	17.74	20.37	15.50	20.03	16.58	19.37
891004	17.48	20.10	15.28	19.78	15.98	19.09
891011	17.68	20.13	15.38	19.89	15.95	19.21
891018	17.64	20.20	15.25	19.89	15.92	19.19
891025	17.34	20.02	14.97	19.73	15.66	19.15
891101	16.65	20.80	14.38	19.10	14.84	18.27
891108	15.95	18.93	13.82	18.44	14.19	17.68
891115	15.37	18.24	13.09	17.83	13.62	17.12
891122	14.48	17.61	12.10	17.08	12.71	16.36
891129	13.27	16.73	11.09	16.20	11.45	15.39
891206	11.89	16.26	9.81	14.89	10.01	13.96
891213	10.48	14.05	8.47	13.24	8.55	12.30
891220	9.23	12.80	7.20	11.18	7.10	10.16
891227	8.21	11.12	6.12	9.33	6.00	8.60
900103	5.48	8.29	5.15	7.83	5.14	7.47
900110	5.07	10.05	4.73	7.47	4.27	6.58
900117	4.30	7.65	3.99	6.36	3.63	5.53
900124	3.53	6.14	3.42	5.33	3.12	4.67
900131	3.28	6.69	3.07	4.82	2.69	4.16
900207	3.06	6.19	2.73	4.42	2.39	3.85
900214	2.75	5.36	2.40	4.17	2.14	3.51
900221	2.64	5.52	2.19	3.98	1.89	3.32
900228	2.68	5.51	2.24	3.92	1.93	3.26
900307	2.67	5.04	2.20	3.91	2.00	3.42
900314	2.99	5.76	2.49	4.39	2.26	3.90
900321	3.36	5.78	2.95	4.95	2.74	4.40
900328	3.98	7.22	3.50	5.75	3.27	5.12
900404	4.56	7.51	4.17	6.42	4.02	5.93

900411	5.06	7.66	4.76	7.04	4.74	6.61
900418	5.74	8.56	5.43	7.72	5.39	7.26
900425	6.34	9.68	6.07	8.54	6.00	8.04
900502	6.73	10.13	6.58	9.17	6.55	8.69
900509	7.14	10.27	7.02	9.68	7.00	9.16
900516	7.69	11.18	7.60	10.52	7.56	9.94
900523	8.38	12.34	8.44	11.22	8.36	10.66
900530	9.11	13.01	9.15	12.11	9.12	11.65
900606	9.86	13.64	9.98	12.92	9.96	12.45
900613	10.23	14.58	10.46	13.69	10.42	13.19
900620	11.16	15.45	11.40	14.67	11.38	14.15
900627	11.77	16.26	12.04	15.38	12.03	14.85